This is non-peer reviewed submitted to EarthArXiv

Exploring the compositional variability of magmas erupted at La Soufrière volcano, St Vincent, using chemostratigraphy and new $^{40}Ar/^{39}Ar$ ages.

Beitris Morrison-Evans[1], Elena Melekhova[1], Richard Robertson[2], Brian Jicha[3], George Cooper[4], Holli Frey[5], Jonathan Blundy[1]

1 University of Oxford, Oxford, UK
2 University of The West Indies, Saint Augustine, Trinidad and Tobago
3 University of Wisconsin-Madison, Madison, US
4 Cardiff University, Cardiff, UK
5 Union College, Schenectady, US

This manuscript is under review at Bulletin of Volcanology

Exploring the compositional variability of magmas erupted at La Soufrière volcano, St Vincent, using chemo-stratigraphy and new $^{40}Ar/^{39}Ar$ ages.

Beitris Morrison-Evans[1]

Elena Melekhova[1]

Richard Robertson[2]

Brian Jicha[3]

George Cooper[4]

Holli Frey[5]

Jonathan Blundy[1]

[1] University of Oxford, Oxford, UK

[2] University of The West Indies, Saint Augustine, Trinidad and Tobago

[3] University of Wisconsin-Madison, Madison, US

[4] Cardiff University, Cardiff, UK

[5] Union College, Schenectady, US

Corresponding author: beitris.morrisonevans@earth.ox.ac.uk

ORCID: 0000-0001-5697-7927

Acknowledgements

We thank the Royal Society for providing funding for a DPhil studentship to BME and a Research Professorship to JB (RP\R1\201048), and a University Research Fellowship to GC (URF\R1\221161). University College Oxford kindly provided part of the funding for BME's fieldwork. We thank Michal Camejo-Harry, Monique Robertson, Tyrone Stafford and Megan Taylor for help during fieldwork and Steve Carey for providing the marine tephra dates.

Abstract

The temporal compositional variation of individual volcanic centres is key to understanding magmatic processes in the underlying crust. La Soufrière volcano, St. Vincent, Lesser Antilles, has erupted predominantly basaltic andesite magmas for hundreds of thousands of years. Sampling of the recently exposed crater walls at La Soufrière reveals that sequentially emplaced crater lavas, feeder dykes, and western flank lavas are low-magnesium basaltic andesites with little variation in major and trace element concentrations, suggesting the system is buffered by the underlying crystal-mush. A single basaltic crater lava unit is more mafic (8 wt. % MgO, 51 – 52 wt. % SiO_2) and is compositionally similar to rare low-magnesium basaltic tephra from large explosive eruptions, suggesting more primitive melts are present in the underlying crust but rarely erupt at the surface. New $^{40}Ar/^{39}Ar$ ages fill a period of previously unaccounted for eruptive history and highlight an unconformity in the crater. A crater lava unit dated at 25.2 ± 3.8 ka is overlain by considerably younger crater lavas dated at 7.9 ± 7.7 and 5.7 ± 4.4 ka. A hornblende-gabbro xenolith is dated at 475.6 ± 28.3 ka, in agreement with early pre-Somma magmatism at La Soufrière volcano, and possibly representing an earlier, now inactive, crystal-mush. Combing new and published data, we show that hiatuses in the geochronological record coincide with major summit collapse events and that the system appears to have stabilised compositionally after the most recent Somma collapse.

Keywords: La Soufrière, crater lavas, basaltic andesite, $^{40}Ar/^{39}Ar$ dating

Introduction

Arc volcanoes can erupt a wide range of magma compositions with compositional diversity observed across entire volcanic island arcs, as well as within individual volcanic centres (e.g. Lesser Antilles: Brown et al., 1977, Melekhova et al., 2015, 2017; Japan: Tatsumi et al., 1994; Kamchatka: Churikova et al., 2001, Koulakov et al., 2017). Some volcanoes, however, repeatedly generate magmas of a near-identical composition over long periods of time (e.g. thousands of years) and are thought to be chemically buffered by the composition of the underlying crustal mush source region (Hildreth and Moorbath, 1988; Blundy, 2022). Examples of volcanoes that erupt magmas with a limited compositional range include Arenal, Costa Rica (Streck et al., 2002, 2005; Parat et al., 2014); North Sister and Mt. Rainer, Cascades (Schmidt and Grunder, 2011; Sisson et al., 2014); Calbuco, Chile (Mixon et al., 2021) and La Soufrière, St. Vincent, Eastern Caribbean (Heath et al., 1998).

La Soufrière erupted most recently in 2020/21 producing near-identical basaltic andesite lava dome-rock and scoria (Weber et al., 2024). These magmas are homogenous yet experienced very different eruptive conditions, making La Soufrière an interesting case study. In this study, we explore the compositional variability of eruptive products from La Soufrière volcano, St. Vincent, to determine how homogenous the magmatic system truly is. By sampling and dating a selection of newly exposed crater lavas, lava flows and dykes, we fill a gap in the eruptive record for La Soufrière and discuss the volcanic history in terms of processes in the underlying source region.

Geological setting

St. Vincent, located at the southern end of the Lesser Antilles volcanic island arc (Fig 1a), is comprised of four main volcanic centres: the Southeast Volcanics field, Grand Bonhomme, Morne Garu and La Soufrière (Fig 1b). La Soufrière is the youngest and currently active volcanic centre, dated at ≤ 0.69 ± 0.09 Ma (Briden et al., 1979). The oldest volcanic rocks on

St. Vincent are 2.74 ± 0.11 Ma from the Southeast Volcanics complex (Briden et al., 1979) and suggest, along with other K-Ar dates (Robertson, 2005) that volcanism has migrated northwards over time. Volcanism on St. Vincent is characterised by alternating periods of effusive and explosive behaviour, ranging from basaltic to andesitic in composition. Feeder dykes are identified at all volcanic centres and lava domes at Grand Bonhomme, Morne Garu and La Soufrière volcanic centres (Rowley, 1978; Sigurdsson, 1981; Robertson, 2002). Plutonic xenoliths at St. Vincent are abundant and include olivine- and amphibole-gabbros, troctolites, olivine-pyroxenites, hornblendites, dunites, wehrlites and websterites (Arculus and Wills, 1980; Tollan et al., 2012; Melekhova et al., 2019; Fedele et al., 2021), revealing the composition of the underlying crystal-rich mush. Calc-silicate xenoliths, including calcareous hornfels and norites are also identified at St. Vincent and suggest magmas are sampling parts of the proto-Caribbean limestone crust (Devine and Sigurdsson, 1980; Camejo-Harry et al., 2024).

La Soufrière volcanic deposits are divided into four main formations based on age: pre-Somma lavas (PSL), yellow tuff formation (YTF), crater lavas (CL) and pyroclastic formation (PF; Rowley, 1978; Sigurdsson, 1981; Heath et al., 1998), followed by two pre-historic (1440 and 1580 CE) and six historic (1718, 1812, 1902/03, 1971/72, 1979 and 2020/21 CE) major eruptions (Cole et al., 2019), each showing some combination of dome-forming and/or explosive activity.

The pre-Somma lavas form the base of the La Soufrière volcano and pre-date the Somma edifice (hence the term ‘pre-Somma’; Heath et al., 1998). The pre-Somma lavas are dated at 0.69 ± 0.09 Ma (K-Ar; Briden et al., 1979) to ≤ 0.18 ± 0.02 Ma ($^{40}Ar/^{39}Ar$; Heath, 1997) and represent at least five-hundred thousand years of effusive volcanism, with few observed intercalated pyroclastic deposits (Sigurdsson, 1981). Collapse of the initial La Soufrière volcano edifice is inferred by a large scarp opening to the west called the Baleine scarp (Fig 1b). Offshore debris avalanche deposits place this flank collapse event at less than 50 ka (Le

Friant et al., 2009). The Somma edifice then grew to the south of this vent before collapsing to the southwest, evidenced by the remaining northern Somma crater wall (Fig 1c) and voluminous debris flows to the southwest (Sigurdsson, 1981). The timing of the Somma collapse is unknown, though one estimate tentatively places it at a few thousand years ago based on eruption rates and the volume of the Somma edifice (Le Friant et al., 2009).

Immediately overlying the Somma collapse debris flows are thick island-wide deposits of the yellow tuff formation (YTF), likely produced by a series of large explosive eruptions (150 m thick in crater, ≤ 5 m thick in Kingstown 20 km south of the crater; Rowley, 1978). Pyroclastic flow deposits that bracket the YTF are radiocarbon dated at 4335 ± 95 yrs and 3590 ± 70 yrs old (Rowley, 1978), constraining the age of the eruptions to within a one-thousand-year window. The crater lavas represent the interior of the youngest and most recent La Soufrière edifice, on the southern rim of the previous Somma edifice. The crater lavas overlie and post-date the YTF and illustrate a second period of continuous effusive volcanism (similar to the pre-Somma lavas), with no visible intercalated ash layers. Activity transitioned to alternating explosive and effusive behaviour known as the pyroclastic formation period, during which the current La Soufrière crater was likely excavated. Today activity continues to alternate between explosive pyroclastic density current (PDC) forming eruptions and effusive lava dome extrusions confined to the crater; products from both eruption types have near-identical compositions (Heath et al., 1998; Cole et al., 2019; Fedele et al., 2021; Weber et al., 2024). The most recent 2020/21 eruption involved the extrusion of a basaltic andesite lava dome, followed by a series of explosive PDC's depositing multiple pyroclastic units (U1 – U5; Cole et al., 2024) and infilling the previous crater.

Previous work

The largest compositional diversity at La Soufrière occurred during early pre-Somma magmatism. Although pre-Somma magmatism is predominantly basaltic andesite (52 – 57 wt.

% SiO_2), a number of high-magnesium basalts (≥ 10 wt. % MgO), low-magnesium basalts (6 – 10 wt. % MgO) and rarer andesites (57 – 60 wt. % SiO_2; Rowley 1978, Heath et al., 1998) are present. The high- and low-magnesium basalts all outcrop along the coastline at the base of the volcano and are inferred to have erupted during building of the initial volcanic edifice (Heath et al., 1998). These basalts match previous St. Vincent basaltic magma compositions from older volcanic centres that were predominantly basaltic (Heath et al., 1998; Robertson, 2002) and illustrate that eruptions of more primitive magmatism declined over time.

Experimental studies exploring the source of the St. Vincent high-magnesium basalts propose that these magmas are derived from two mantle-wedge sources: 1.3 GPa, 1225ºC with 2 wt. % H_2O, and 1.6 GPa, 1185ºC with 4.5 wt. % H_2O. The oxygen fugacity for these primitive magmas is estimated to be between NNO+1 to NNO+2.3, (Pichavant et al., 2002, Pichavant and Macdonald, 2007, Melekhova et al., 2015). These high-magnesium basalts are proposed to differentiate at different depths within the crust to form low-magnesium basalts, high-aluminium basalts, basaltic andesites and andesites (Melekhova et al., 2015). Of these magmas, basaltic andesites are by far the most frequently erupted composition at La Soufrière (Rowley, 1978; Heath et al., 1998), yet their source depth and environment within the crust have been little explored.

Lava samples from the old Somma edifice, collected by Rowley (1978) from the extant northern wall are basaltic andesite to andesite, with the more evolved compositions interpreted as effusive lava flows that never reached the coastline. Previous sampling of the current La Soufrière crater lavas revealed predominantly basaltic andesite compositions (Rowley, 1978), with a small number of andesitic lavas in the eastern wall and three andesitic dykes crosscutting the crater lavas, all of which are now buried by the 2020/21 pyroclastic deposits. All eruption products since 1440 CE are basaltic andesite, with the exception of six low-magnesium basaltic tephra samples from the 1902/03 eruption (Cole et al., 2019).

By exploring geochemical trends in a series of sequentially emplaced effusive crater lavas at La Soufrière volcano, and in dykes and lava flows from the western flanks of the volcano, we aim to determine whether La Soufrière reflects a long-lived homogenous basaltic andesite magmatic system with little compositional variation, or whether La Soufrière magmas experience different degrees of chemical modification, such as fractionation, magma mixing or sediment assimilation. Dating a selection of these samples constrains the timing of emplacement, furthering our understanding of the eruptive history of the currently active La Soufrière volcanic centre and how magma chemistry has changed over time.

Methods

Fieldwork

The 2020/21 eruption at La Soufrière exposed the previously heavily vegetated crater walls, providing a unique opportunity for sampling. The crater lavas were emplaced successively, thus preserving their relative stratigraphic sequence, which is ideal for evaluating sequential changes in geochemistry and petrology. Rowley (1978) collected rocks from lower down in the crater lava sequence but was unable to reach the upper crater lava units. The 2020/21 eruption deposited up to 100 m of ash within the crater, burying the lowermost crater lavas, but provided access to the upper units (Fig 2). In 2023 a team from the University of Oxford, University of Cardiff and the University of the West Indies sampled the crater lavas. Sixteen individual crater lava units in the northeast to southeast walls were identified (Fig 2a), with samples collected from thirteen.

The YTF produced thick pyroclastic deposits with lithic-rich layers containing dense blocks of lava. Six lava blocks were collected from within a 15 m thick deposit of the YTF exposed on the east coast, just north of North Union (Fig 1b, 3c), to compare with the composition of the crater lavas and determine if the YTF was emplaced simultaneously to the crater lavas, or if the lava blocks represent older lavas (e.g. Somma or pre-Somma lavas).

In 2024 we returned to the field to sample newly exposed lava flows and dykes on the western flanks after the 2020/21 explosive eruptions cleared out much of the vegetation. Nine lava samples and five dyke samples were collected from Larikai and Roseau valley. All sample names and locations are reported in Table 1. An adcumulate hornblende-gabbro sample (VSG-2), collected loose from Jacobs Well during a field campaign in 2009, was also dated.

Whole-rock geochemistry

Forty-one samples were powdered (see appendix for details) for whole-rock major and trace element analysis using the geofacilities laboratories at the Department of Earth Sciences, University of Oxford. These samples include nineteen crater lavas, seven lava blocks recovered from the YTF, six samples from lava flows in Larikai valley, three samples from lava flows in Roseau valley, five samples from two different dykes and one sample of loose dome-rock (age unknown) collected in the current crater. Major elements were analysed by x-ray fluorescence (XRF) following a lithium-borate fusion and trace elements were analysed by inductively coupled plasma mass spectrometry (ICP-MS) at ALS Geochemistry, Loughrea, Ireland. Precision of analyses were 2 % for major elements and 10 % for trace element measurements. Results are reported in Tables 1 and 2.

Trace element data for the U5 scoria from the 2021 explosive eruption are also presented here for comparison. 200 g of the U5 scoria was dissolved into solution and analysed using an 8900 Agilent ICP-MS at the Department of Geoscience, Union College (see appendix for details). Major element data for these samples was previously reported in Weber et al. (2024).

$^{40}Ar/^{39}Ar$ dating

Nine lava samples, a dyke sample and a xenolith were selected for $^{40}Ar/^{39}Ar$ dating. The criteria for the sample selection included minimal alteration and low vesicularity. Sample preparation occurred at the Department of Geoscience, University of Wisconsin-Madison. Samples were crushed, sieved and ultrasonically leached in 3M HCl for 15 minutes, followed

by thorough and repeated rinsing with deionised water. Purification of the groundmass by magnetic sorting and hand-picking removed phenocrysts, xenocrysts and any altered material, to leave only fresh groundmass material (180 – 250 μm grainsize). Samples were then loaded into aluminium foil packets and irradiated in the cadmium-lined in-core tube at the Oregon State University reactor. The 1.1864 Ma Alder Creek sanidine standard was irradiated simultaneously to monitor the neutron flux (Jicha et al., 2016).

Analysis of the irradiated samples was completed at the WiscAr Laboratory at the University of Wisconsin-Madison. Samples were incrementally heated by a CO_2 laser to release the gas trapped in the sample in stages. The gas was then cleaned to remove H_2O, H_2, O_2, CO_2, CH_4, and CO, and analysed on an Isotopx NGX-600 mass spectrometer at 650 μA to determine isotopic abundances. $^{40}Ar/^{39}Ar$ ages were then calculated using the decay constant from Min et al. (2000) and an atmospheric ratio of 298.5 ± 0.31 $^{40}Ar/^{36}Ar$, as determined by Lee et al. (2006). Heating steps that caused an increase in mean standard weight deviation (MSWD) ≥ 1.5 were excluded from the calculated ages (Powell et al., 2002; Jicha et al., 2016) and are shown in the plateau diagrams in the supplementary material (Fig S1). The inverse isochrons all have intercepts that are within uncertainty of the atmospheric value, indicating that excess Ar is not present. Therefore, the plateau ages reported in Table 3 are used in the subsequent discussion.

Results

Fieldwork

Field observations confirm the sequential emplacement of the crater lavas (e.g. filling of topographic lows, lack of well-defined interstitial ash layers), with thicker units displaying shearing (Fig 3a). The relative age order of the crater lavas is presented in Figures 2 and 8.

The lava flows in Larikai and Roseau valley are often extensive, interbedded with debris flows, and display shearing in thicker flows (Fig 3g). A 15 m tall and 10 m wide dyke was identified crosscutting the lower Larikai lavas (Lower Larikai (LL) dyke; Fig 3d), and a 15 m tall, 70 m long dyke striking 300º outcropped to the NW of the crater in the upper Larikai valley, intersecting the Somma crater wall (Upper Larikai (UL) dyke; Fig 3e). The crater lavas and lava flows in Larikai and Roseau valley contained abundant igneous and calc-silicate xenoliths (e.g. Fig 3i), and a large multi-textural xenolith block was identified in Roseau valley (Fig 3h) providing evidence for the crystal-rich mush that underlies the volcano.

Whole-rock major element chemistry

New whole-rock major element data are reported in Table 1. Compositions range from basalt to andesite (49.5 – 57.5 wt. % SiO_2), with most lavas sitting in the basaltic andesite field (Fig 4). Three crater lava samples have considerably higher magnesium (~8 wt. % MgO) and lower silica (~51 – 52 wt. % SiO_2) contents (Fig 5a) and are hereafter referred to as the mafic crater lava unit (units 9 and 11 of Fig 2 combined based on stratigraphic positioning) and are similar in composition to previously identified low-magnesium basalts (Robertson, 2002). The YTF lava blocks are distinctive with lower SiO_2 and NaO_2 and higher CaO and Al_2O_3 contents than the main cluster of whole-rock data (Fig 5).

The new lava data presented in this study are all calcium and aluminium rich (~8 – 11 wt. % CaO; ~17 – 20 wt. % Al_2O_3; Fig 5b-c), characteristic of the southern Lesser Antilles arc (e.g. MacDonald et al., 2000). High calcium contents denote a delay in clinopyroxene fractionation (Stamper et al., 2014; Klein et al., 2023), whilst high aluminium contents indicate supressed plagioclase fractionation due to high dissolved water contents (Sisson and Grove, 1993; Pichavant and Macdonald, 2007). Iron and titanium (7 – 9 wt. % FeO_T; 0.7 – 1.2 wt. % TiO_2) remain fairly constant relative to MgO contents of lavas. A rapid decrease in iron and titanium in melt inclusion (MI) data at ≤ 2 wt. % MgO (Fig 5f, g) is a trend unique to St. Vincent

compared to the other islands in the arc (Smith et al., 1980). New data follow typical differentiation trends and are in good agreement with previous whole-rock data for La Soufrière and older St. Vincent volcanic centres. Melt inclusions show wider chemical diversity than whole-rock compositions, with a noticeable deviation above 7 wt. % MgO to low SiO_2, high CaO and TiO_2, and pronounced scatter at low MgO, particularly for alkalis and TiO_2.

Trace element geochemistry

Trace element concentrations and trace element ratios are reported in Table 2. Trace element concentrations are enriched by approximately one order of magnitude relative to the primitive mantle (Sun and McDonough, 1989). Rare Earth Element (REE) plus Sr, Zr and Hf patterns appear relatively flat and strikingly parallel with little variation between lava samples and agree with previous St. Vincent data (grey shading, Fig 6). The mafic crater lavas generally have the lowest REE concentrations supporting their more primitive nature. Data show a positive Sr anomaly (~200 – 250 ppm Sr; Fig 6, Table 2) despite a small negative Eu anomaly, characteristic of arc magmas (Turner and Langmuir, 2022). Two of the YTF lava blocks display significantly higher Sr peaks (460 ppm Sr; STV_LS_21 and 26) and depletions in LREE (La-Sm) and Zr relative to other samples; these are the same lava blocks with elevated Ca and Al contents.

Eu/Eu* ratios (where $Eu^* = Eu_N / \sqrt{Gd_N * Sm_N}$) for the La Soufrière magmas range from 0.8 to 1 (Fig 7a) and tentatively decrease with differentiation, as illustrated by increasing La. The weak negative Eu anomaly is indicative of a low proportion of Eu^{2+} partitioning into plagioclase (where plagioclase proportions are similar, as in these magmas) and therefore a higher magmatic oxidation state (Aigner-Torres et al, 2007). Elevated fO_2 can account for the observed decoupling of Sr and Eu (Fig 6), which are ordinarily both compatible in plagioclase. For example, at ≥ QFM +2 less than 10 % of Eu is divalent (Aigner-Torres et al., 2007).

The Dy/Dy* ratio (where $Dy^* = Dy_N / \sqrt{Gd_N^{4/13} * Sm_N^{9/13}}$; Davidson et al., 2013) is used to distinguish between garnet fractionation, that preferentially uptakes HREE, and amphibole or clinopyroxene fractionation that prefer MREE. Dy/Dy* values for the La Soufrière lavas are positively correlated with Dy/Yb and support amphibole or clinopyroxene fractionation (Davidson et al., 2013) consistent with the subtle spoon-shaped pattern of MREE in Figure 6. The negative relationship between Dy/Dy* and La (Fig 7b) suggests evolved magmas experienced more amphibole or clinopyroxene fractionation. Amphibole fractionation is consistent with the abundance of amphibole (and plagioclase) rich cumulates at St. Vincent (Tollan et al., 2012).

$^{40}Ar/^{39}Ar$ ages

New $^{40}Ar/^{39}Ar$ ages for seven lava samples and a xenolith from La Soufrière are reported in Table 3 and their stratigraphic context shown schematically in Figure 8 (unsuccessful ages reported in appendix). $^{40}Ar/^{39}Ar$ age spectra and inverse isochron plots for all samples are reported in the supplementary materials. Dates agree with estimated stratigraphic positions from field observations. Three of four crater lavas were successfully dated. Crater lava STV_LS_46 (unit 14) in the southeastern crater wall is dated at 7.9 ± 7.7 ka, and STV_LS_6 (unit 7) in the eastern crater wall is 5.7 ± 4.4 ka (Fig 2a). The high uncertainty associated with these young dates, due to low abundances of K_2O (Fig 5e) and hence radiogenic Ar, means determining the exact emplacement chronology and drawing conclusions about the morphology of the crater is not possible, but it does confirm their relative young age. The lowermost crater lava unit sampled (STV_LS_5a) is dated at 25.2 ± 3.8 ka and sits at the relative base of the new outer crater in the northern wall (unit 10; Fig 2a). Previously the crater lavas had been estimated at ~4 ka by association with the YTF eruption (Rowley, 1978; Heath, 1997; Robertson 2002), however our new ages show that the lower crater lavas are significantly older than the upper crater lavas, suggesting either a hiatus in activity or that the older crater lavas originate from an earlier phase of volcanism (e.g. Somma).

New dates for the lavas in Larikai valley range from 33.7 ± 8.0 to 4.4 ± 4.2 ka and in Roseau valley from 31.5 ± 4.0 to 14.5 ± 3.1 ka (Fig 8). These dates are considerably younger than previously dated pre-Somma lavas on the eastern flanks (Table 4), though overlap with a lava from the southeastern flanks that could have originated from either Morne Garu or La Soufrière (11 ± 14 ka, Table 4; Heath, 1997; Robertson, 2005). The youngest lower Larikai lava (4.4 ± 4.2 ka; STV_LS_103) is crosscut by a dyke (Fig 3d), meaning effusive activity continued on the western flank after 4 ka, possibly coeval to the emplacement of the crater lavas. Further work is needed to constrain the relationship between the younger lower Larikai lava flow, the crosscutting dyke and the emplacement of the crater lavas.

The hornblende-gabbro xenolith sample (VSG-2; amph+plag+ol) gave a considerably older age of 475.6 ± 28.3 ka, corresponding to much earlier pre-Somma magmatism. This date records when the xenolith ceased exchanging argon with the atmosphere, perhaps due to cooling and/or lack of melt present, but not its original formation.

Discussion

Compositional variation at La Soufrière volcano

All dated eruption products (this study and literature data) from La Soufrière are arranged in stratigraphic order (Fig 9a) using radiocarbon, marine fossil, K-Ar and $^{40}Ar/^{39}Ar$ dates, as well as observed stratigraphic positions to assess chemical variation over time and the presence of any hiatuses that could record perturbations to the magmatic system. The YTF tephra are shown out of sequence as field observations place the YTF below the upper crater lavas stratigraphically (Sigurdsson, 1981). Radiocarbon dating of tephra samples extends back to ~5 ka (Rowley, 1978; Robertson, 1992; Heath, 1997; Cole et al., 2019), whilst K-Ar and $^{40}Ar/^{39}Ar$ dating of pre-Somma lavas collected from the flanks of the volcano range from 690 – 180 ka (Table 4; Briden et al., 1979; Heath, 1997; Robertson, 2002). Marine tephra from St. Vincent occurs in drill cores GS-27 and EN-46 in the Grenada basin, and were correlated to

St. Vincent using geochemical fingerprinting (Carey, 1992). Dates for these units were calculated using sedimentation rates and the boundary defining the disappearance of planktonic foraminifera in the *Globorotalia medarii* complex at the end of the last ice age (12 ka; Sigurdsson and Carey, 1981; Reid et al., 1996). Table 4 lists the depths of the St. Vincent units in these drill cores and their corresponding ages (0.6 – 18 ka). The Baleine collapse is estimated at ~50 ka from offshore debris avalanche deposits and sedimentation rates (Le Friant et al., 2009), with the Somma collapse clearly postdating this event (see collapse scarps Fig 1b). Le Friant et al. (2009) suggest the Somma collapse occurred approximately a few thousand years ago based on average eruption rates and volumes, however this does not constrain the timing of the event very well. The Somma collapse has previously been tentatively linked to the YTF eruption (3.6 – 4.3 ka; Rowley, 1978; Sigurdsson, 1981; Heath et al., 1998) and must have occurred prior to the emplacement of the La Soufrière crater lavas that sit in the depression formed by the collapse.

When arranged in stratigraphic sequence (Fig 9a) the samples show a number of gaps where there are few if any dates. Given the relative completeness of the stratigraphic and radiometric catalogue, it is reasonable to assume that these gaps may correspond to hiatuses in the eruption record. The most prominent gap is observed between 33.7 ± 8 and 180 ± 21 ka (Table 4). Although this gap was apparent from literature data prior to our study, the new $^{40}Ar/^{39}Ar$ ages from Roseau and Lower Larikai narrow the gap. This gap brackets the postulated age for the Baleine collapse, suggesting that either this event removed part of the stratigraphic record or occurred during a period of volcanic quiescence.

There is less geochronological evidence for the poorly dated Somma collapse. There is a gap in the marine tephra record between 3.1 and 15 ka with the younger tephra plausibly corresponding to the YTF. In terms of on-land volcanic rocks there is a marked break in the crater lava sequence between 25.2 ± 3.8 ka (unit 10 of Fig 2a) and the overlying upper crater lavas at ≤ 8 ka. A single lava flow from Roseau (STV_LS_167) was emplaced within this time

gap at 14.5 ± 3.1 ka. The uncertainties on our $^{40}Ar/^{39}Ar$ ages of the upper crater lavas (5.7 ± 4.4 ka and 7.9 ± 7.7 ka; units 7 and 14) do not enable us to establish if they pre-date or post-date the YTF (4.3 to 3.6 ka; Rowley, 1978), but field relationships strongly suggest the latter, hence the stratigraphic sequence shown in Figure 9a.

Figure 9b shows the compositional variation over the same stratigraphic sequence, highlighting the chemical uniformity of the La Soufrière magmatic system from ~34 ka onwards (lilac triangles upwards), with rare low-magnesium (6 – 10 wt. % MgO) basalts erupted during the YTF, crater lava period and in 1902/03. Note that the marine tephra are glasses rather than whole-rocks, so are not considered as representative bulk magma chemistry. Compositions for magmas whose relative but not absolute ages are known are shown as square symbols to display the full chemical diversity at La Soufrière. No sequential geochemical trends are observed in the crater lavas and the limited variation in major and trace element compositions (Fig 4 – 7) attests to a long-lived, homogenous period of volcanism with magmas tapping into a chemically-buffered source region (Blundy, 2022). The single exception is a mafic crater lava (units 9 and 11 combined; Fig 2a) with 8 wt. % MgO (blue circle in Fig 9b). The pre-Somma lavas cluster at basaltic andesite but extend to high-magnesium basalts and show similar chemical variations to earlier volcanic centres on St. Vincent. Previous studies (e.g. Heath et al., 1998) suggest more primitive volcanism decreased, and eventually ceased, over time at La Soufrière. However, it is possible that the high-magnesium pre-Somma basalts (orange squares and triangles with ≥ 10 wt. % MgO; Fig 9b) may instead be lava flows from the previous volcanic centre Morne Garu (Fig 1b), upon which La Soufrière grew. Lavas from the Somma crater walls (lilac squares Fig 9b; Rowley, 1978) are similar to the new data presented in this study and previously sampled crater lavas, suggesting the magmatic system had homogenised by the time the Somma edifice grew. One hypothesis is that the large flank collapse eruption that formed the Baleine scarp could have resulted in major changes in the magma plumbing system and subsequent stabilisation of erupted magma compositions as observed on Montserrat (Cassidy et al., 2015), St. Eustatius

(Roobol and Smith, 2004), and St. Lucia (Boudon et al., 2013). There is however 146 kyr of eruptive activity that remains unaccounted for, during which the Baleine collapse occurred, and where the variation of magma compositions (if erupted) are unknown.

Five of the YTF lava blocks sampled in this study are geochemically distinct, with elevated CaO and Al_2O_3 and lower SiO_2 and Na_2O than other La Soufrière lavas (Fig 5). Two of the YTF lava blocks (STV_LS_22 and 24) also have high Sr (Fig 6). Elevated Sr and Ca have previously been associated with two different magma types, M- and C-series, in Grenada and the Grenadines (Stamper et al., 2014; White et al., 2017; Melekhova et al., 2022), which also seem to be present in St. Vincent. High-Ca magmas have not previously been reported at St. Vincent but are observed in the melt inclusion record (Fig 5), supporting the presence of Ca-rich melts in the subsurface. These anomalous lava blocks were erupted during the highly explosive YTF eruption and may represent a previously unsampled part of the La Soufrière magmatic system.

The hornblende-gabbro xenolith dated in this study corresponds in age to the pre-Somma lavas at 476 ka (Fig 9a), suggesting it represents a fragment of the crystal-mush that was active at the time. Recently identified micro-xenoliths in erupted scoria samples from historic and pre-historic La Soufrière have gabbroic mineral assemblages containing abundant orthopyroxene, but lacking amphibole and olivine (Fedele et al., 2021), suggesting the underlying crystal-mush may have changed in composition over time such that these younger xenoliths represent the currently active system, or sections of the mush not previously sampled. Melekhova et al. (2019) have shown that the mineralogy of plutonic xenoliths in the Lesser Antilles is controlled by P-T-H_2O-fO_2 conditions in the subsurface. Thus, changes in magma source depths and temperatures over time may be reflected in changes in xenolith mineralogy.

Differentiation from a basaltic parent magma

Melekhova et al. (2015) suggest that the basaltic andesite magmas of St. Vincent are generated by polybaric differentiation of a high-magnesium, mantle-derived, basaltic parent melt in the lower crust, between 0.7 – 1 GPa and ~1050ºC, and low-magnesium basalts from the same parent melt but deeper and hotter, 1 – 1.3 GPa and 1050 – 1100ºC. High-magnesium basalts erupted more frequently from older volcanic centres on St. Vincent and during the early pre-Somma period but became rarer with time (Heath et al., 1998), with the most recent high-magnesium basalt erupting from La Soufrière 180 ka (Fig 9b). Over time La Soufrière's source depth appears to have shallowed, and for the last few tens of thousands of years the volcano has been fed primarily from the basaltic andesite magma source, occasionally erupting low-magnesium basalts and andesites, but no mantle-derived high-magnesium basalts.

The relatively flat and enriched REE patterns observed for the La Soufrière basaltic andesite magmas, with respect to the primitive mantle (Fig 6), support a small degree of coherent differentiation from a mantle-derived parent. Eu/Eu* and Dy/Dy* ratios decrease with differentiation (Fig 7) and support plagioclase and amphibole fractionation, respectively (Davidson et al., 2013). The trend is only weakly defined for plagioclase fractionation; likely a consequence of fractionation at oxidising conditions (Drake and Weill, 1975). High water contents can create more oxidising conditions and can contribute to forming the high-An plagioclase ubiquitous in erupted cumulates from St. Vincent (Sisson and Grove, 1993; Tollan et al., 2012; Fedele et al., 2021). St. Vincent magmas are known to be fluid-rich based on H_2O contents and $\delta^{11}B$ compositions in mineral-hosted melt inclusions (Bouvier et al., 2008; Cooper et al., 2020) and high Ba/Th ratios (Atlas et al., 2022). Previous experimental studies also support a hydrous and oxidised source for the parent melt (Pichavant et al., 2002; Melekhova et al., 2015). Amphibole is absent from the phenocryst assemblage in La Soufrière magmas, as is common in many volcanoes undergoing cryptic amphibole fractionation (Davidson et al., 2007), but is abundant in cumulates. Amphibole is only stable at higher water contents (Krawczynski et al., 2012) providing further evidence for a water-rich source region.

Trace element ratios (e.g. Th/Nb, La/Sm, Th/Yb; Table 2) attest to low sediment input and little crustal contamination (Hawksworth et al., 1991, Plank and Langmuir, 1993; Elliot, 2003; Atlas et al., 2022), as do $^{87}Sr/^{86}Sr$ ratios that remain similar to the mantle (0.7040; Pushkar et al.,1973), suggesting erupted magmas at St. Vincent represent relatively unmodified liquids extracted from the crust.

Low-magnesium basalts of La Soufrière

The mafic crater lava is a low-magnesium basalt and similar in major element geochemistry to mafic tephra from the 1902/03 eruption (Heath et al., 1998; Cole et al., 2019), a mafic pumice from the YTF eruption (STV376; Heath et al., 1998) and two low-magnesium pre-Somma lavas (STV309 and STV315; Heath et al., 1998) (Fig 5). The mafic crater lava (units 9 and 11; Fig 2a) is the only effusive low-magnesium basalt to be identified within the current La Soufrière crater.

Limited trace element data exist for the YTF tephra and pre-Somma lava samples for comparison, but Rb, Ba, Sr, Zr and Y concentrations in the samples mentioned above generally agree within error with the mafic crater lava. The mafic YTF tephra has higher Nb (3.7 vs 2.2 ppm) and Cr (557 vs 364 ppm) than the mafic crater lavas, the low-magnesium basalt pre-Somma lava STV315 has lower La (3.2 vs 4.6 ppm) and Ce (8 vs 11 ppm) whilst STV309 has lower V (215 vs 303 ppm) compared to the mafic crater lava. Trace element data for recent pyroclastic deposits (Cole et al., 2019) show the mafic 1902/03 tephra are in very good agreement with the mafic crater lava trace element concentrations, but are slightly elevated in LREE (e.g. 5.5 vs 4.6 ppm La) and vary in V and Cr concentrations. Cr, however, notably varies within the mafic crater lava samples by ~90 ppm, possibly reflecting Cr-spinel fractionation or other Cr-rich mineral phases such as olivine and clinopyroxene (Barnes and Roeder, 2001). In general, the low-magnesium basalts of La Soufrière are compositionally

very similar over a wide time interval suggesting they could be sourced from similar physico-chemical conditions in the crust.

The 1902/03 eruption is the largest historically reported eruption at La Soufrière, generating large eruption columns, PDC's and ashfall (Carey and Sigurdsson, 1978; Rowley, 1978; Shepherd et al., 1979). There was no confirmed effusive counterpart to this eruption, and the eruption evolved from basaltic andesite to basaltic over its course. The presence of two discrete magma compositions within the 1902/03 eruption has previously been interpreted as the emptying of a zoned magma chamber (Roobol and Smith, 1975), today considered a zoned crystal-mush or melt lens (Edmonds et al., 2019); or to reflect mafic injection possibly responsible for triggering the eruption (Cole et al., 2019). The 1902/03 eruption has many similarities to the YTF eruption and could represent a smaller version of the YTF eruption. The mafic crater lava is too high up the stratigraphic sequence to be related to the YTF eruption, thus may correspond to expulsion of vestigial mafic melts from a dominantly basaltic andesite system.

Revised stratigraphic sequence

Pre-Somma lavas

The pre-Somma lavas represent the earliest and compositionally most diverse magmas at La Soufrière that now form the base of the volcanic edifice (Fig 9 and 10). Pre-Somma magmatism is dated at 690 to 180 ka, there is then a gap in the eruptive history from 180 to 34 ka (Table 4). The Baleine collapse is estimated at 50 ka (Le Friant et al., 2009) and we cannot discount the possibility that the Baleine collapse removed some of the intervening volcanic record, with the collapse removing much of the main volcanic edifice, allowing the Somma edifice to begin growing. The magmatic system appears to stabilise from this point onwards (Fig 9b) with only basaltic andesites and rare low-magnesium basalts erupted.

Somma lavas and Somma collapse

The age of the Somma edifice and date of the Somma collapse are unknown, however new $^{40}Ar/^{39}Ar$ ages and stratigraphic observations presented in this study provide some insight. The lowermost crater lava collected in this study (unit 10; Fig 2a) is dated at ~25 ka, considerably older than previous estimates for the crater lavas (~4 ka; Heath, 1997) and new ages for the upper crater lavas (≤ 8 ka) emplaced ≤ 30 m above (Fig 3b), highlighting a major unconformity in the crater. The 25 ka lower crater lava could represent part of the Somma crater that survived the collapse, a slumped Somma lava block, or evidence a hiatus in the crater lava sequence. The 25 ka crater lava is similar in major and trace element geochemistry to many La Soufrière lavas, including the previously sampled Somma lavas and the younger upper crater lavas (Fig 5), meaning geochemistry cannot be used to distinguish the origin of the lower crater lavas. Collapse of the Somma edifice must precede the crater lavas as they fill the depression created by the collapse of the edifice to the south. The collapse would have blocked the existing vent, causing magmas to find a new route to the surface, as is common at volcanoes that experience repetitive edifice or flank collapse (e.g. Martinique, Tenerife, El Hierro; Maccaferri et al., 2017), resulting in the new vent location for the current La Soufrière edifice.

YTF eruption

The collapse of the Somma crater has previously been linked to the YTF eruption due to YTF deposits immediately overlying the Somma collapse debris flow deposits, with no evidence of erosion (Rowley, 1978; Sigurdsson, 1981). Additionally, such a large collapse, illustrated by the tall remnant northern crater wall and inferred material removed would have likely resulted in considerable depressurisation of the system and triggered a large explosive eruption (Manconi et al., 2009; Cassidy et al., 2018) supported by the thick and widespread YTF eruption deposits (Rowley, 1978), with lithic-rich layers containing lava blocks ≥ 70 cm (Fig

3c). Two pyroclastic flows that overlie and underlie the YTF are radiocarbon dated and constrain the age of the eruption to be between 4.3 and 3.6 ka (Rowley, 1978). These dates coincide with the onset of the extrusion of the upper crater lavas (Fig 9) and support the 25 ka lower crater lava to be a relict lava block from the Somma crater.

Crater lavas

New $^{40}Ar/^{39}Ar$ ages for two crater lavas (5.9 ± 4.4 and 7.9 ± 7.7 ka) and one of the youngest crater lavas (≤ 4 ka) without any detectable radiogenic Ar, agree with previous estimates that the crater lavas are young and overlap in age with YTF eruption (≤ 4.3 ka; Rowley, 1978; Sigurdsson, 1981; Heath, 1997). Previous eruptive histories propose volcanic activity during the emplacement of the crater lavas was constrained to the crater, however the young lava flow in Larikai valley (4.4 ± 4.2 ka) suggests otherwise. Sigurdsson (1981) also identified thin lenses of lava flows between debris flows to the south of the crater, but was unable to constrain their ages to during or after the YTF eruption. The young Larikai lava flow sits on top of a debris flow and is crosscut by a dyke (Fig 3d), implying volcanism on the western flank of La Soufrière was still occurring until much more recently than previously thought. The crater lavas exposed today comprise the eastern wall of the current crater (Fig 2), suggesting there must have been an opening for these lavas to flow down at the time. Previous mapping in the La Soufrière crater also identified truncated lava flows and infilling of older smaller summit vents (Rowley, 1978), suggesting that explosive eruptions have continued to play a significant role in controlling the morphology of the crater.

Pyroclastic formation and historic lavas

The pyroclastic formation of La Soufrière's volcanic history, which post-dates the YTF, is comprised of alternating explosive and effusive eruptions. Historical eruptions mostly encompassed both effusive and explosive volcanism, with the effusive volcanism confined to the crater, today defined by a 100 – 200 m deep depression, and often involving the extrusion

of relatively small viscous lava domes. It is unclear when effusive magmatism evolved from voluminous lava flows to small viscous lava domes, as compositionally these magmas are identical. The change could represent a difference in volume of material available, magma ascent rate or viscosity (Cassidy et al., 2018). The explosive eruptions during the pyroclastic formation phase are likely responsible for forming the general crater morphology observed today and carving out the vent magmas erupt from. What is clear, however, is that the explosive and effusive phases have near-constant chemistry for almost 4 kyr, suggestive of sourcing from a stable, chemically-buffered magma reservoir at depth.

Conclusions

We demonstrate that magmas erupted from La Soufrière over the last 34 kyr are predominantly basaltic andesite with very limited major and trace element chemical variation. Elevated REE concentrations and trace element ratios indicate that these magmas experienced a small degree of coherent differentiation, fractionating plagioclase and amphibole at hydrous and oxidising conditions. These observations agree with previous experimental studies that found basaltic andesite magmas on St. Vincent to be generated by polybaric differentiation at lower crustal conditions from a mantle-derived, high-magnesium basalt parent (Melekhova et al., 2015). Trace element ratios suggest low sediment or crustal input into the magmas.

A single low-magnesium basalt crater lava unit (~8 wt. % MgO) is identified and is more primitive than all other crater lavas. This unit is geochemically similar to a small number of previously reported mafic tephra in the YTF and 1902/03 deposits, and low-magnesium basaltic pre-Somma lavas. These rare mafic pyroclastic products correlate with two of the largest explosive eruptions at La Soufrière (YTF and 1902/03). Collapse of the Somma edifice likely triggered the YTF eruption by rapid depressurisation of the magmatic system. Such large-scale eruptions can result in deeper more primitive magma sources being tapped

(Manconi et al., 2009), as was observed in the 1902/03 eruption (Roobol and Smith, 1975). Further work is required to establish the eruption conditions during the emplacement of the mafic crater lava.

New $^{40}Ar/^{39}Ar$ ages for lavas erupted from La Soufrière fill a gap in the eruptive history record and reveal four key findings. Firstly, a major gap in the stratigraphic sequence between 34 and 180 ka straddles the postulated age of the Baleine collapse (~50 ka). The 33.7 ± 8 ka lava from Lower Larikai likely marks the onset of renewed volcanism following collapse. Secondly, an unconformity is identified in the northern wall of the current crater where the oldest crater lava (25.2 ± 3.8 ka) is overlain by crater lavas that are considerably younger (7.9 ± 7.7 and 5.7 ± 4.4 ka) and coeval with the YTF. The anomalously old crater lava could represent a vestigial part of the Somma crater that survived the Somma collapse or even a slumped lava block of Somma lava. Thirdly, dates for lavas exposed on the western flanks of La Soufrière range from 33.7 ± 8 ka to 4.4 ± 4.2 ka. The youngest lava flow in the lower Larikai valley is crosscut by a dyke, suggesting volcanism on the western flank of La Soufrière continued until more recently than previously thought, possibly coeval with the emplacement of the crater lavas. Effusive volcanism since then has produced lava domes refined to the crater. Finally, an erupted xenolith from La Soufrière is dated at 475.6 ± 28.3 ka, in agreement with early pre-Somma magmatism and could represent a fragment of the underlying crystal-mush that is no longer active.

The compositional consistency of La Soufrière basaltic andesite magmas is suggestive of a long-lived, chemically-buffered source region, whose mineralogy corresponds to that of erupted plutonic xenoliths. Reactions between the mush and interstitial melts may have provided this buffering, as envisaged by Blundy (2022). Less-evolved, low-magnesium basalt magmas may occur locally within the source region, but only become liberated and erupted during major perturbations to the systems, such as the two well-documented collapse events, or major explosive eruptions, such as that in 1902/03.

Acknowledgements

We thank the Royal Society for providing funding for a DPhil studentship to BME and a Research Professorship to JB (RP\R1\201048), and a University Research Fellowship to GC (URF\R1\221161). University College Oxford kindly provided part of the funding for BME's fieldwork. We thank Michal Camejo-Harry, Monique Robertson, Tyrone Stafford and Megan Taylor for help during fieldwork and Steve Carey for providing the marine tephra dates.

Funding

This work was supported by the Royal Society (RP\R1\201048 and URF\R1\221161). University College, Oxford provided additional funding for fieldwork.

Declaration

Competing interests

The authors declare no competing interests.

Author contributions

Conceptualisation: [EM, RR, JB, BM-E]; Methodology: [BM-E, EM, JB]; Investigation [BM-E, EM, GC, RR]; Formal analysis: [BM-E, BJ, HF]; Writing - original draft preparation: [BM-E]; Writing - review and editing: [BME, JB, EM, GC, RR, BJ, HF]; Visualisation [BM-E]; Funding acquisition: [JB, GC]; Supervision: [JB, EM].

Appendices

Extended methods

Rock powder preparation

Rock powder preparation for all samples collected in this study were performed at the University of Oxford. Lava samples were initially split into smaller fragments (≤ 5 cm^3) and any alteration removed using the stainless-steel rock splitter. Samples were then washed in an ultrasonic bath for 10 minutes and left to dry overnight in a 40ºC oven. Approximately 200 g of the clean sample material was crushed to ≤ 1 mm using the jaw crusher, where a stainless-steel fixed-jaw and removeable-jaw crush the material in one mm intervals, from 5 mm to ≤ 1 mm. The crushed material was then poured through a stainless-steel sample splitter at least three times to ensure a homogenous and representative batch of material.

Grinding of a sample material to a fine powder was carried out using either the agate ball mill or Tema mill. I used both for time efficiency. The ball mill contains four agate holders, each containing 10 agate balls, allowing four samples to be powdered simultaneously. 40 g of sample material was weighed into each agate holder and run at 400 rpm for 20 minutes. The Tema mill contains an inner and outer agate ring. Again 40 g of sample material was added to the agate container and run for 10-20 minutes until a fine powder obtained. Approximately 10 g of each rock powder was weighed into a glass vial and sent to ALS Geochemistry, Loughrea, Ireland for whole-rock major and trace element analysis.

All equipment was cleaned with compressed air and ethanol between each sample, the mills were also run with cleaning silica between samples to reduce contamination. The extractor fan in the preparation laboratory was ran during crushing and cleaning to keep the air clean, and gloves were worn to further reduce contamination.

U5 scoria preparation

Trace elements of the U5 scoria bulk rock were prepared and analysed at Union College. For each analysis, 200 mg of powdered sample was weighed into a PicoTrace (Bovendan, Germany) Teflon bomb system. Four standards were used for calibration. The powders were dissolved through several steps. Rock powders were dissolved in 0.5 mL of 50% HF and heated to 180ºC for four days, and then allowed to cool and evaporate at 100ºC. 15 mL of 70% HNO_3 was then added and allowed to evaporate again. A mixture of 125 mL HNO_3, 25 mL of 37% HCl, 2 mL of HF, and 0.3 mL of 1000 ng/g internal standards including Rh, In, Re, and Bi were diluted to 500 mL and 15 mL added to each sample. The Teflon crucibles were sealed and heated to 150ºC overnight. Once cooled, 0.2 mL of each sample solution and 10 mL of 1% HNO_3 was added to 12 mL test tubes for analysis.

Dilute samples were analysed on an Agilent 8900 ICP-QQQ Triple-Quad Mass Spectrometer in No-Gas mode for the lightest and heaviest elements (Li, Be, Pb, Th, U), in O_2 gas mode for V, Cr, Co, Sb and REEs, and in He gas mode for all others. Powdered natural reference materials from 3 basalts and 1 rhyolite, NIST (688, 278) and the USGS (BIR-1, BCR-2), were used for standardisation. To check method accuracy USGS basalt standard BHVO-2 was run as an unknown, and measured compositions match known values within 5 % for all elements, with the exception of Mo, Sn, and Sb which are generally within 20 %.

Unsuccessful $^{40}Ar/^{39}Ar$ dates

One crater lava (STV_LS_ 11; unit 4) close to the top of the crater lava sequence gave a negative age due to its recent eruption and high ^{36}Ar content (likely ≤ 4 ka). Crater lava STV_LS_3 (unit 1) sits stratigraphically above STV_LS_11, so it was not dated. The Upper Larikai dyke gave a staircase-upwards plateau spectrum indicative of excess ^{40}Ar (Schaen et al., 2020).

References

Aigner-Torres M, Blundy J, Ulmer P, Pettke T (2007) Laser Ablation ICPMS study of trace element partitioning between plagioclase and basaltic melts: an experimental approach. Contrib Mineral Petrol 153:647–667. https://doi.org/10.1007/s00410-006-0168-2

Arculus RJ, Wills KJA (1980) The Petrology of Plutonic Blocks and Inclusions from the Lesser Antilles Island Arc. Journal of Petrology 21:743–799. https://doi.org/10.1093/petrology/21.4.743

Atlas ZD, Germa A, Boss B, et al (2022) Variable element enrichment sources and contributions to volcanic rocks along the Lesser Antilles Island Arc. Front Earth Sci 10:782179. https://doi.org/10.3389/feart.2022.782179

Bardintzeff JM (1983) Les verres et les magmas de l'eruption 1979 de la Soufriere de Saint-Vincent (Antilles). Bulletin de la Société Géologique de France S7-XXV:811–818. https://doi.org/10.2113/gssgfbull.S7-XXV.6.811

Bardintzeff J-M (1984) Les pyroxènes et leurs inclusions, marqueurs privilégiés des nuées ardentes (Saint-Vincent, Antilles, 1979). bulmi 107:41–54. https://doi.org/10.3406/bulmi.1984.7792

Barnes SJ, Roeder PL (2001) The Range of Spinel Compositions in Terrestrial Mafic and Ultramafic Rocks. Journal of Petrology 42:2279–2302. https://doi.org/10.1093/petrology/42.12.2279

Blundy J (2022) Chemical Differentiation by Mineralogical Buffering in Crustal Hot Zones. Journal of Petrology 63:egac054. https://doi.org/10.1093/petrology/egac054

Boudon G, Villemant B, Friant AL, et al (2013) Role of large flank-collapse events on magma evolution of volcanoes. Insights from the Lesser Antilles Arc. Journal of Volcanology and Geothermal Research 263:224–237. https://doi.org/10.1016/j.jvolgeores.2013.03.009

Bouvier A-S, Métrich N, Deloule E (2008) Slab-Derived Fluids in the Magma Sources of St. Vincent (Lesser Antilles Arc): Volatile and Light Element Imprints. Journal of Petrology 49:1427–1448. https://doi.org/10.1093/petrology/egn031

Briden JC, Rex DC, Faller AM, Tomblin JF (1979) K-Ar geochronology and palaeomagnetism of volcanic rocks in the Lesser Antilles island arc. Phil Trans R Soc Lond A 291:485–528. https://doi.org/10.1098/rsta.1979.0040

Brown GM, Holland JG, Sigurdsson H, et al (1977) Geochemistry of the Lesser Antilles volcanic island arc. Geochimica et Cosmochimica Acta 41:785–801. https://doi.org/10.1016/0016-7037(77)90049-7

Camejo-Harry M, Melekhova E, Aufrère S, et al (2024) Early arc crust formation preserved in the Grenadines archipelago, southern Lesser Antilles arc. R Soc Open Sci 11:231914. https://doi.org/10.1098/rsos.231914

Carey S (1992) Studies on the Generation, Dispersal and Deposition of Tephra in the Marine and Terrestrial Environment. PhD Thesis, Universiry of Rhode Island

Carey SN, Sigurdsson H (1978) Deep-sea evidence for distribution of tephra from the mixed magma eruption of the Soufrière on St. Vincent, 1902: Ash turbidites and air fall. Geol 6:271. https://doi.org/10.1130/0091-7613(1978)6<271:DEFDOT>2.0.CO;2

Cassidy M, Cole PaulD, Hicks KE, et al (2015) Rapid and slow: Varying magma ascent rates as a mechanism for Vulcanian explosions. Earth and Planetary Science Letters 420:73–84. https://doi.org/10.1016/j.epsl.2015.03.025

Cassidy M, Manga M, Cashman K, Bachmann O (2018) Controls on explosive-effusive volcanic eruption styles. Nat Commun 9:2839. https://doi.org/10.1038/s41467-018-05293-3

Churikova T, Dorendorf F, Wörner G (2001) Sources and Fluids in the Mantle Wedge below Kamchatka, Evidence from Across-arc Geochemical Variation. Journal of Petrology 42:1567–1593. https://doi.org/10.1093/petrology/42.8.1567

Cole PD, Barclay J, Robertson REA, et al (2024) Explosive sequence of La Soufrière, St Vincent, April 2021: insights into drivers and consequences via eruptive products. SP 539:81–106. https://doi.org/10.1144/SP539-2022-292

Cole PD, Robertson REA, Fedele L, Scarpati C (2019) Explosive activity of the last 1000 years at La Soufrière, St Vincent, Lesser Antilles. Journal of Volcanology and Geothermal Research 371:86–100. https://doi.org/10.1016/j.jvolgeores.2019.01.002

Cooper GF, Macpherson CG, Blundy JD, et al (2020) Variable water input controls evolution of the Lesser Antilles volcanic arc. Nature 582:525–529. https://doi.org/10.1038/s41586-020-2407-5

Davidson J, Turner S, Handley H, et al (2007) Amphibole “sponge” in arc crust? Geol 35:787. https://doi.org/10.1130/G23637A.1
Davidson J, Turner S, Plank T (2013) Dy/Dy*: Variations Arising from Mantle Sources and Petrogenetic Processes. Journal of Petrology 54:525–537. https://doi.org/10.1093/petrology/egs076
Devine JD, Sigurdsson H (1980) Garnet–fassaite calc-silicate nodule from La Soufrière, St. Vincent. American Mineralogist 65:302–305
Dostal J, Dupuy C, Carron JP, et al (1983) Partition coefficients of trace elements: Application to volcanic rocks of St. Vincent, West Indies. Geochimica et Cosmochimica Acta 47:525–533. https://doi.org/10.1016/0016-7037(83)90275-2
Drake MJ, Weill DF (1975) Partition of Sr, Ba, Ca, Y, Eu2+, Eu3+, and other REE between plagioclase feldspar and magmatic liquid: an experimental study. Geochimica et Cosmochimica Acta 39:689–712. https://doi.org/10.1016/0016-7037(75)90011-3
Edmonds M, Cashman KV, Holness M, Jackson M (2019) Architecture and dynamics of magma reservoirs. Phil Trans R Soc A 377:20180298. https://doi.org/10.1098/rsta.2018.0298
Elliott T (2003) Tracers of the slab. In: Eiler J (ed) Geophysical Monograph Series. American Geophysical Union, Washington, D. C., pp 23–45
Fedele L, Cole PD, Scarpati C, Robertson REA (2021) Petrological insights on the last 1000 years of explosive activity at La Soufrière volcano, St. Vincent (Lesser Antilles). Lithos 392:106150. https://doi.org/10.1016/j.lithos.2021.106150
Graham AM, Thirlwall MF (1981) Petrology of the 1979 eruption of Soufriere volcano, St. Vincent, Lesser Antilles
Hawkesworth CJ, Hergt J, Ellam R, McDermott F (1991) Element fluxes associated with subduction related magmatism. Phil Trans R Soc Lond A 335:393–405. https://doi.org/10.1098/rsta.1991.0054
Heath E (1997) Genesis and evolution of calc-alkaline magmas at Soufriere volcano, St. Vincent, Lesser Antilles arc. PhD Thesis, Lancaster University
Heath E, Macdonald R, Belkin H, et al (1998) Magmagenesis at Soufrière Volcano, St Vincent, Lesser Antilles Arc. Journal of Petrology 39:1721–1764. https://doi.org/10.1093/petroj/39.10.1721
Hildreth W, Moorbath S (1988) Crustal contributions to arc magmatism in the Andes of Central Chile. Contr Mineral and Petrol 98:455–489. https://doi.org/10.1007/BF00372365
Jicha BR, Singer BS, Sobol P (2016) Re-evaluation of the ages of 40Ar/39Ar sanidine standards and supereruptions in the western U.S. using a Noblesse multi-collector mass spectrometer. Chemical Geology 431:54–66. https://doi.org/10.1016/j.chemgeo.2016.03.024
Klein BZ, Jagoutz O, Schmidt MW, Kueter N (2023) A Global Assessment of the Controls on the Fractionation of Arc Magmas. Geochem Geophys Geosyst 24:e2023GC010888. https://doi.org/10.1029/2023GC010888
Koulakov I, Abkadyrov I, Al Arifi N, et al (2017) Three different types of plumbing system beneath the neighboring active volcanoes of Tolbachik, Bezymianny, and Klyuchevskoy in Kamchatka. JGR Solid Earth 122:3852–3874. https://doi.org/10.1002/2017JB014082
Krawczynski MJ, Grove TL, Behrens H (2012) Amphibole stability in primitive arc magmas: effects of temperature, H2O content, and oxygen fugacity. Contrib Mineral Petrol 164:317–339. https://doi.org/10.1007/s00410-012-0740-x
Lacroix A (1949) Sur des enclaves endopolygènes de Saint-Vincent. bulmi 72:571–590. https://doi.org/10.3406/bulmi.1949.4686
Le Bas MJ, Maitre RWL, Streckeisen A, et al (1986) A Chemical Classification of Volcanic Rocks Based on the Total Alkali-Silica Diagram. Journal of Petrology 27:745–750. https://doi.org/10.1093/petrology/27.3.745
Le Friant A, Boudon G, Arnulf A, Robertson REA (2009) Debris avalanche deposits offshore St. Vincent (West Indies): Impact of flank-collapse events on the morphological evolution of the island. Journal of Volcanology and Geothermal Research 179:1–10. https://doi.org/10.1016/j.jvolgeores.2008.09.022
Lee J-Y, Marti K, Severinghaus JP, et al (2006) A redetermination of the isotopic abundances of atmospheric Ar. Geochimica et Cosmochimica Acta 70:4507–4512. https://doi.org/10.1016/j.gca.2006.06.1563
Maccaferri F, Richter N, Walter TR (2017) The effect of giant lateral collapses on magma pathways and the location of volcanism. Nat Commun 8:1097. https://doi.org/10.1038/s41467-017-01256-2
Macdonald R, Hawkesworth CJ, Heath E (2000) The Lesser Antilles volcanic chain: a study in arc magmatism. Earth-Science Reviews 49:1–76. https://doi.org/10.1016/S0012-8252(99)00069-0

Manconi A, Longpre M-A, Walter TR, et al (2009) The effects of flank collapses on volcano plumbing systems. Geology 37:1099–1102. https://doi.org/10.1130/G30104A.1

Melekhova E, Blundy J, Martin R, et al (2017) Petrological and experimental evidence for differentiation of water-rich magmas beneath St. Kitts, Lesser Antilles. Contrib Mineral Petrol 172:98. https://doi.org/10.1007/s00410-017-1416-3

Melekhova E, Blundy J, Robertson R, Humphreys MCS (2015) Experimental Evidence for Polybaric Differentiation of Primitive Arc Basalt beneath St. Vincent, Lesser Antilles. Journal of Petrology 56:161–192. https://doi.org/10.1093/petrology/egu074

Melekhova E, Schlaphorst D, Blundy J, et al (2019) Lateral variation in crustal structure along the Lesser Antilles arc from petrology of crustal xenoliths and seismic receiver functions. Earth and Planetary Science Letters 516:12–24. https://doi.org/10.1016/j.epsl.2019.03.030

Min K, Mundil R, Renne PR, Ludwig KR (2000) A test for systematic errors in 40Ar/39Ar geochronology through comparison with U/Pb analysis of a 1.1-Ga rhyolite. Geochimica et Cosmochimica Acta 64:73–98. https://doi.org/10.1016/S0016-7037(99)00204-5

Mixon EE, Singer BS, Jicha BR, Ramirez A (2021) Calbuco, a monotonous andesitic high-flux volcano in the Southern Andes, Chile. Journal of Volcanology and Geothermal Research 416:107279. https://doi.org/10.1016/j.jvolgeores.2021.107279

Nakamura N (1974) Determination of REE, Ba, Fe, Mg, Na and K in carbonaceous and ordinary chondrites. Geochimica et Cosmochimica Acta 38:757–775. https://doi.org/10.1016/0016-7037(74)90149-5

Parat F, Streck MJ, Holtz F, Almeev R (2014) Experimental study into the petrogenesis of crystal-rich basaltic to andesitic magmas at Arenal volcano. Contrib Mineral Petrol 168:1040. https://doi.org/10.1007/s00410-014-1040-4

Pichavant M, Macdonald R (2007) Crystallization of primitive basaltic magmas at crustal pressures and genesis of the calc-alkaline igneous suite: experimental evidence from St Vincent, Lesser Antilles arc. Contrib Mineral Petrol 154:535–558. https://doi.org/10.1007/s00410-007-0208-6

Pichavant M, Mysen BO, Macdonald R (2002) Source and H2O content of high-MgO magmas in island arc settings: an experimental study of a primitive calc-alkaline basalt from St. Vincent, lesser antilles arc. Geochimica et Cosmochimica Acta 66:2193–2209. https://doi.org/10.1016/S0016-7037(01)00891-2

Plank T (2005) Constraints from Thorium/Lanthanum on Sediment Recycling at Subduction Zones and the Evolution of the Continents. Journal of Petrology 46:921–944. https://doi.org/10.1093/petrology/egi005

Plank T, Langmuir CH (1993) Tracing trace elements from sediment input to volcanic output at subduction zones. Nature 362:739–743. https://doi.org/10.1038/362739a0

Powell R, Hergt J, Woodhead J (2002) Improving isochron calculations with robust statistics and the bootstrap. Chemical Geology 185:191–204. https://doi.org/10.1016/S0009-2541(01)00403-X

Pushkar P, Steuber AM, Tomblin JF, Julian GM (1973) Strontium isotopic ratios in volcanic rocks from St. Vincent and St. Lucia, Lesser Antilles. J Geophys Res 78:1279–1287. https://doi.org/10.1029/JB078i008p01279

Reid R, Carey SN, Ross DR (1996) Late Quaternary sedimentation in the Lesser Antilles island arc. Geological Society of America Bulletin 108:78–100. https://doi.org/10.1130/0016-7606(1996)108<0078:LQSITL>2.3.CO;2

Robertson R (2002) The Volcanic Geology of the Pre- Soufrière Rocks of St. Vincent, West Indies. PhD Thesis, University of the West Indies

Robertson REA (2005) Volcanic hazard atlas of the Lesser Antilles: St. Vincent. In: Volcanic hazard atlas of the Lesser Antilles. Seismic Research Unit, The University of the West Indies, Trinidad and Tobago, pp 239–261

Roobol MJ, Smith AL (1975) A Comparison of the Recent Eruptions of Mt. Pelee, Martinique and Soufriere, St. Vincent

Roobol MJ, Smith AL (2004) Volcanology of Saba and St. Eustatius Northern Lesser Antilles. Royal Netherlands Academy of Arts and Sciences (Koninklijke Nederlandse Akademie Van Wetenschappen)

Rowley K (1978) Stratigraphy and geochemistry of the Soufriere volcano, St. Vincent, West Indies. PhD Thesis, University of the West Indies St. Augustine - Seismic Research Unit

Schmidt ME, Grunder AL (2011) Deep Mafic Roots to Arc Volcanoes: Mafic Recharge and Differentiation of Basaltic Andesite at North Sister Volcano, Oregon Cascades. Journal of Petrology 52:603–641. https://doi.org/10.1093/petrology/egq094

Shepherd JB, Aspinall WP, Rowley KC, et al (1979) The eruption of Soufrière volcano, St Vincent April–June 1979. Nature 282:24–28. https://doi.org/10.1038/282024a0

Sigurdsson H (1981) Geologic Observations in the crater of Soufrière volcano, St. Vincent. University of the West Indies, Seismic Research Unit, Special Publication.

Sigurdsson H, Carey SN (1981) Marine Tephrochronology and Quaternary Explosive Volcanism in the Lesser Antilles Arc. In: Self S, Sparks RSJ (eds) Tephra Studies. Springer Netherlands, Dordrecht, pp 255–280

Sisson TW, Grove TL (1993) Experimental investigations of the role of H20 in calc-alkaline differentiation and subduction zone magmatism

Sisson TW, Salters VJM, Larson PB (2014) Petrogenesis of Mount Rainier andesite: Magma flux and geologic controls on the contrasting differentiation styles at stratovolcanoes of the southern Washington Cascades. Geological Society of America Bulletin 126:122–144. https://doi.org/10.1130/B30852.1

Smith AL, Roobol MJ, Gunn BM (1980) The lesser antilles — A discussion of the Island arc magmatism. Bull Volcanol 43:287–302. https://doi.org/10.1007/BF02598033

Stamper CC, Blundy JD, Arculus RJ, Melekhova E (2014) Petrology of Plutonic Xenoliths and Volcanic Rocks from Grenada, Lesser Antilles. Journal of Petrology 55:1353–1387. https://doi.org/10.1093/petrology/egu027

Streck MJ, Dungan MA, Bussy F, Malavassi E (2005) Mineral inventory of continuously erupting basaltic andesites at Arenal volcano, Costa Rica: implications for interpreting monotonous, crystal-rich, mafic arc stratigraphies. Journal of Volcanology and Geothermal Research 140:133–155. https://doi.org/10.1016/j.jvolgeores.2004.07.018

Streck MJ, Dungan MA, Malavassi E, et al (2002) The role of basalt replenishment in the generation of basaltic andesites of the ongoing activity at Arenal volcano, Costa Rica: evidence from clinopyroxene and spinel. Bull Volcanol 64:316–327. https://doi.org/10.1007/s00445-002-0209-2

Sun S, McDonough WF (1989) Chemical and isotopic systematics of oceanic basalts: implications for mantle composition and processes. SP 42:313–345. https://doi.org/10.1144/GSL.SP.1989.042.01.19

Tang M, Ji W-Q, Chu X, et al (2021) Reconstructing crustal thickness evolution from europium anomalies in detrital zircons. Geology 49:76–80. https://doi.org/10.1130/G47745.1

Tatsumi Y, Furukawa Y, Yamashita S (1994) Thermal and geochemical evolution of the mantle wedge in the northeast Japan arc: 1. Contribution from experimental petrology. J Geophys Res 99:22275–22283. https://doi.org/10.1029/94JB00283

Thirlwall MF, Smith TE, Graham AM, et al (1994) High Field Strength Element Anomalies in Arc Lavas: Source or Process? Journal of Petrology 35:819–838. https://doi.org/10.1093/petrology/35.3.819

Tollan PME, Bindeman I, Blundy JD (2012) Cumulate xenoliths from St. Vincent, Lesser Antilles Island Arc: a window into upper crustal differentiation of mantle-derived basalts. Contrib Mineral Petrol 163:189–208. https://doi.org/10.1007/s00410-011-0665-9

Turner SJ, Langmuir CH (2022) Sediment and ocean crust both melt at subduction zones. Earth and Planetary Science Letters 584:117424. https://doi.org/10.1016/j.epsl.2022.117424

Weber G, Blundy J, Barclay J, et al (2024) Petrology of the 2020–21 effusive to explosive eruption of La Soufrière Volcano, St Vincent: insights into plumbing system architecture and magma assembly mechanism. SP 539:171–200. https://doi.org/10.1144/SP539-2022-177

White W, Copeland P, Gravatt DR, Devine JD (2017) Geochemistry and geochronology of Grenada and Union islands, Lesser Antilles: The case for mixing between two magma series generated from distinct sources. Geosphere 13:1359–1391. https://doi.org/10.1130/GES01414.1

Figures

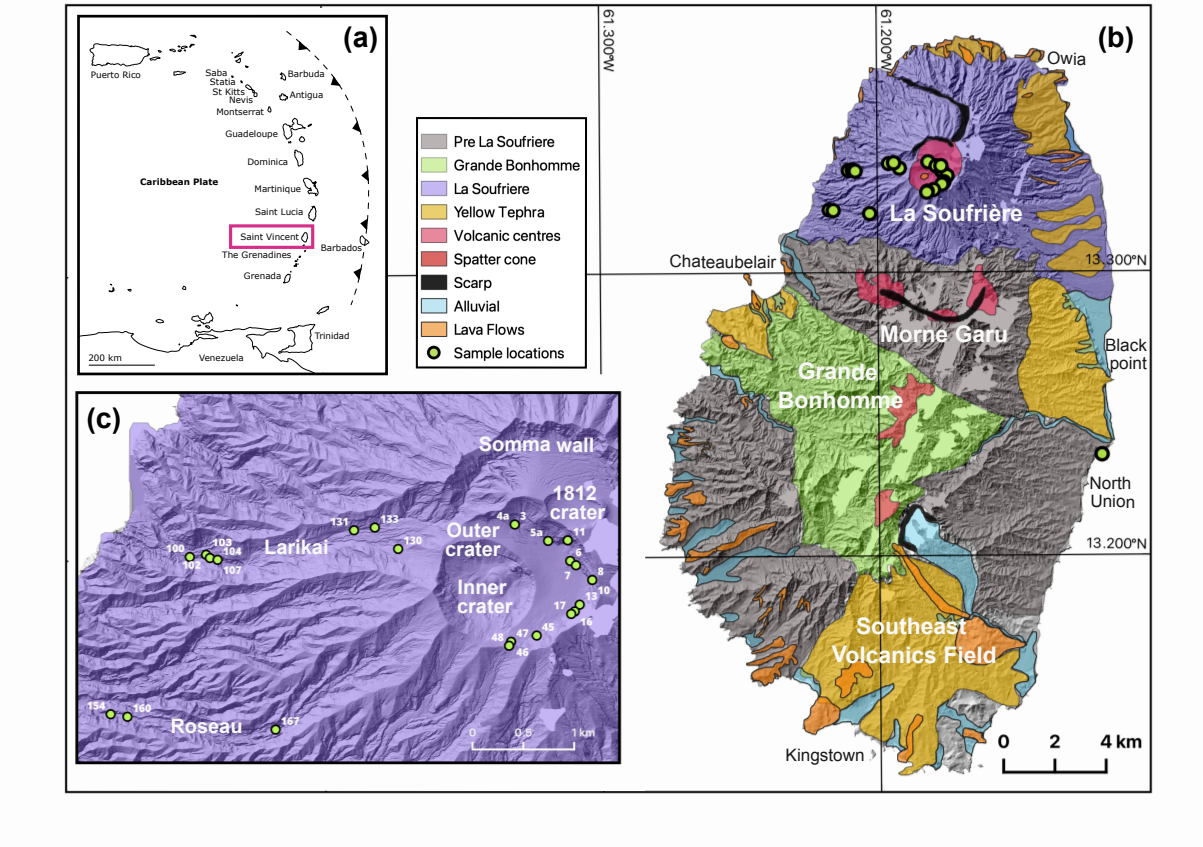

Fig 1 Map of **(a)** the Lesser Antilles volcanic island arc and **(b)** the island of St. Vincent. The four volcanic centres present on St. Vincent are labelled, with La Soufrière being the youngest and currently active. Geological units after Robertson (2005). Digital elevation model data from USGS-VDAP. **(c)** Inset map showing sample numbers and locations in La Soufrière crater and Larikai and Roseau valley, as listed in Table 1 (e.g. STV_LS_3 shown as number 3).

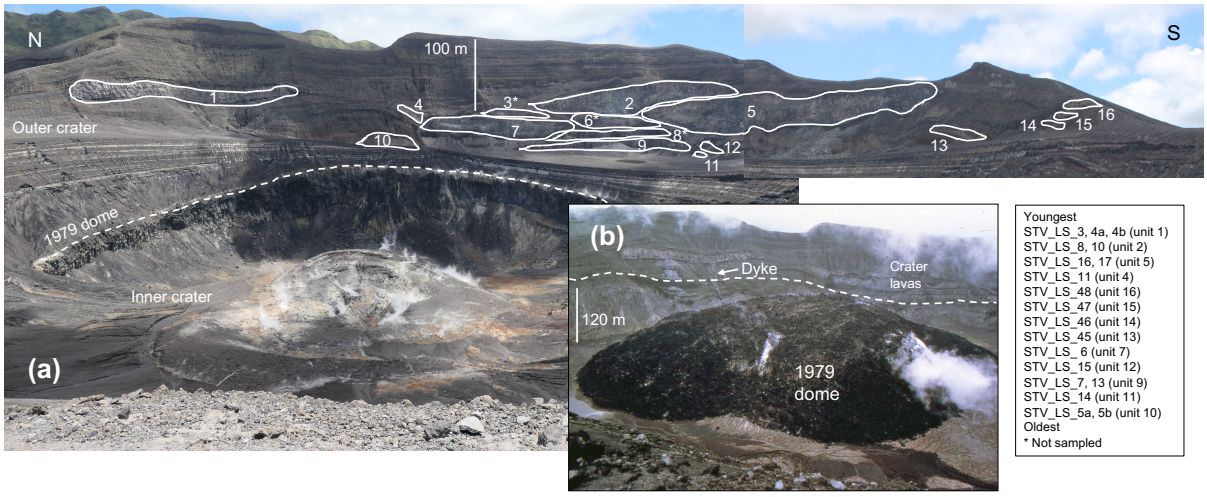

Fig 2 (a) Photograph of La Soufrière crater lava units sampled during fieldwork in 2023. Unit numbers assigned in the field. Crater lava units ordered from youngest to oldest based on stratigraphic position. Dashed line shows upper surface of 1979 dome with radial jointing and interior now exposed. **(b)** Photograph of the 1979 dome and lower crater lava units. Dashed line represents the floor of the outer crater today, below which is now infilled with pyroclastic material from the 2020/21 eruption. Photograph (a) taken in 2023 and (b) in 1983 (by Fiske, Smithsonian), both facing east.

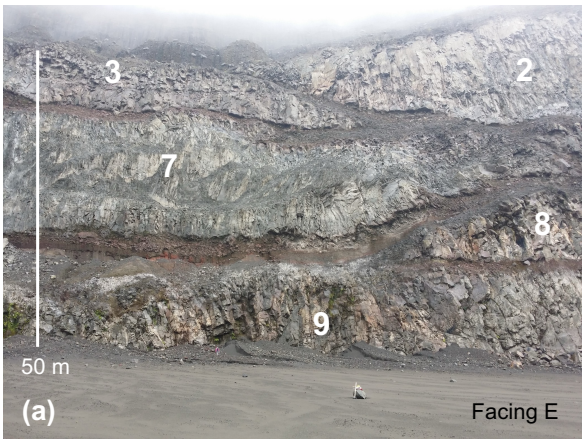
3
2
7
8
9
50 m
(a)
Facing E

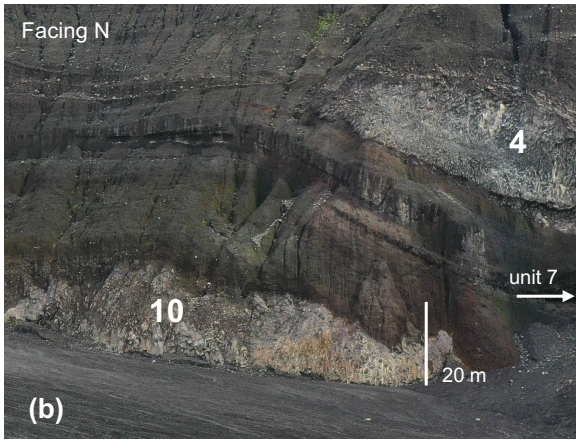
Facing N
4
unit 7
10
20 m
(b)


YTF
5 m
(c)
Facing W

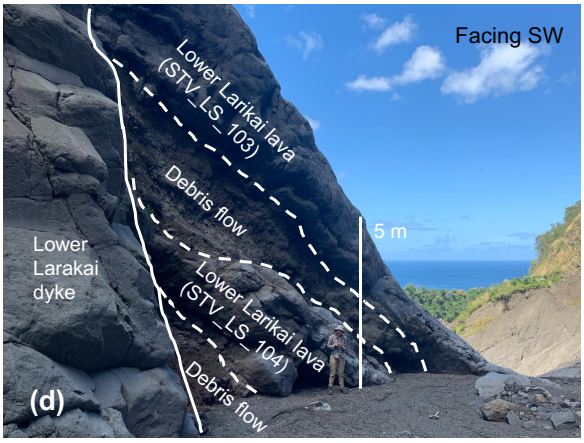
Facing SW
Lower Larikai lava (STV_LS_103)
Debris flow
Lower Larakai dyke
Lower Larikai lava (STV_LS_104)
Debris flow
5 m
(d)

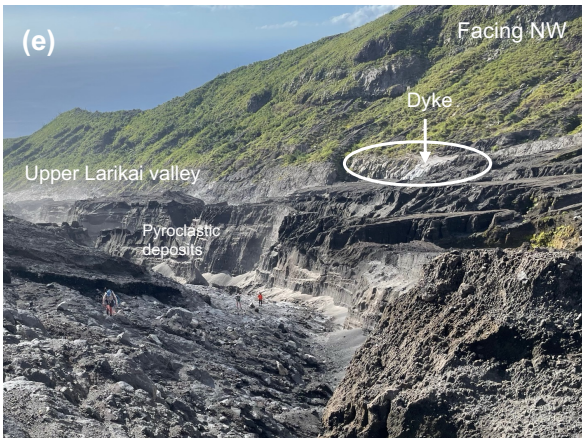
(e)
Facing NW
Dyke
Upper Larikai valley
Pyroclastic deposits

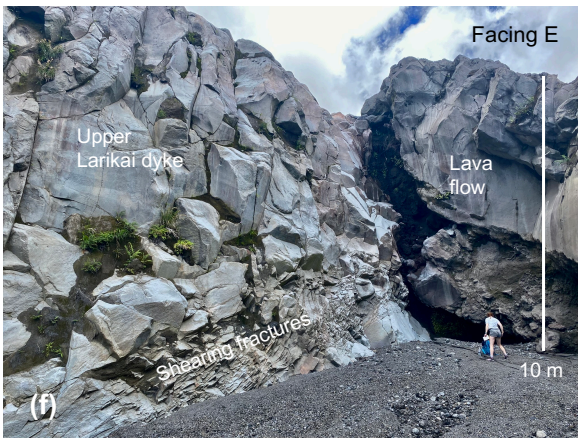
Facing E
Upper Larikai dyke
Lava flow
Shearing fractures
10 m
(f)

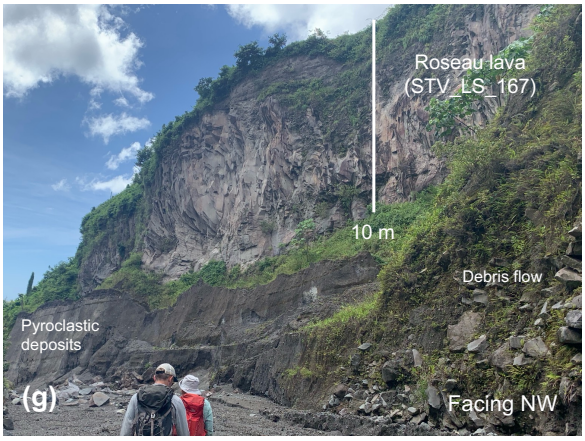
Roseau lava (STV_LS_167)
10 m
Debris flow
Pyroclastic deposits
(g)
Facing NW


1 m
(h)

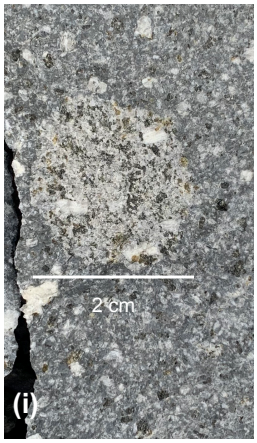
2 cm
(i)

Fig 3 (a) Crater lavas in the eastern wall with unit numbers labelled. Lavas display lens-like morphologies and are separated by red rubbly surfaces. Jointing observed within all lava flows and shearing at the centre of thicker flows (e.g. unit 7). Pyroclastic unit continues above unit 3. **(b)** Crater lavas in northeastern wall. Top of unit 10 exposed and covered in thick pyroclastic deposits. Unit 4 is a considerably younger upper crater lava emplaced ≤ 30 m above unit 10. **(c)** 15 m thick YTF deposit displaying layering and containing large lithic lava blocks (≤ 70 cm) near North Union (see Fig 1b). **(d)** Lava flows in lower Larikai valley interbedded with debris flows and cross cut by a vertical dyke. **(e)** Upper Larikai valley with a dyke exposed on the northern side of the valley (circled). Lavas in the background covered by vegetation are likely the Somma lavas comprising the still standing northern Somma crater wall. Thick pyroclastic deposits in the valley make access to lavas difficult. **(f)** Contact between Upper Larikai dyke and lava flow. Upward tilt of lava flow and shearing fractures at the base of the exposure clearly observed. **(g)** Thick lava flow in Roseau valley (STV_LS_167) with sheared interior exposed. **(h)** Giant xenolith block from Roseau valley predominantly composed of interlocking plagioclase, clinopyroxene and olivine crystals. Clusters of different mineral assemblages observed, some displaying layering and banding (circled). **(i)** In-situ micro-xenolith (≤ 3 cm) in lower Larikai lava STV_LS_100. Contains plagioclase and olivine and displays a recrystallised darker core.

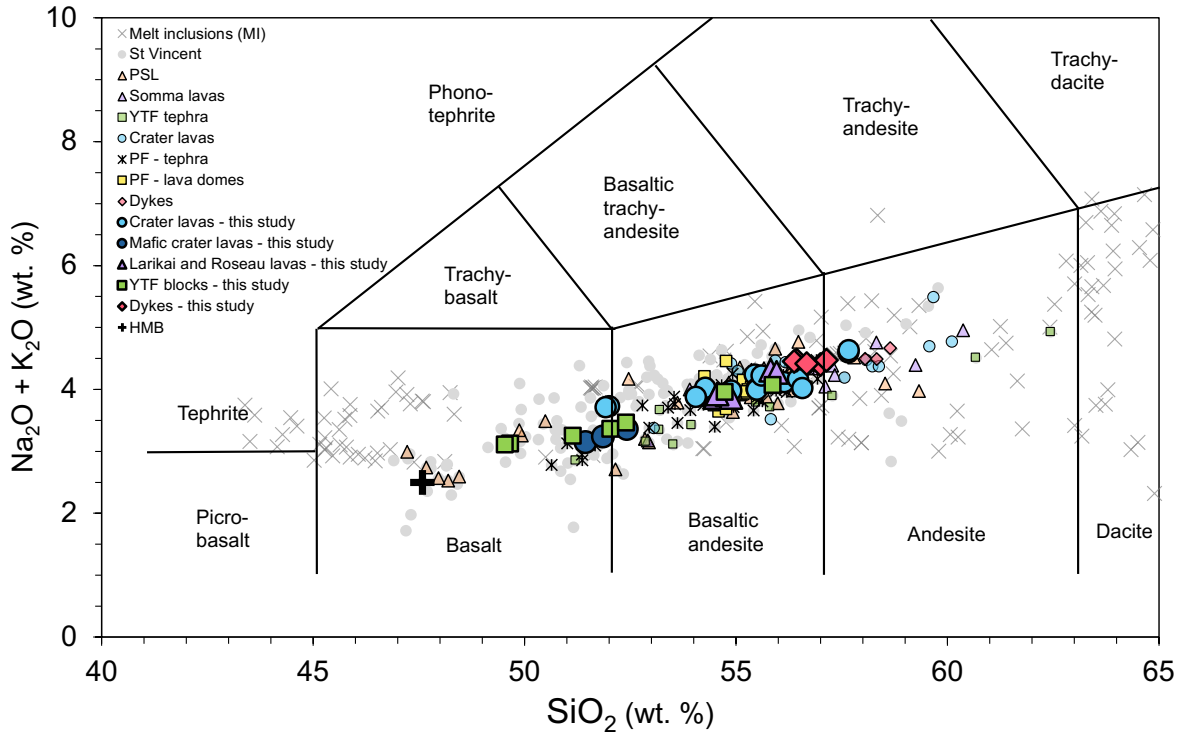

Fig 4 Total alkali versus silica (TAS) diagram after Le Bas et al. (1986). PSL – pre-Somma lavas; Somma lavas include Larikai and Roseau lavas; CL – crater lavas; YTF – yellow tuff formation; PF - pyroclastic formation. New data for samples analysed in this study are shown as large bold symbols with thick outlines, previous data for La Soufrière eruption products are shown as smaller faded symbols (Rowley, 1978; Heath et al., 1998; Cole et al., 2019). Previous data for lavas and melt inclusions (MI) from older volcanic centres on St. Vincent are shown as grey circles and crosses (data from Robertson 2002 and GEOROC: Lacroix, 1949; Bardintzeff et al., 1983, 1984; Graham and Thirlwall, 1981; Dostal et al., 1983; Thirlwall et al., 1994; Heath et al., 1998; Plank, 2005; Cole et al., 2019; Fedele et al., 2021). A high-magnesium basalt (HMB; RSV49; Robertson 2002) is shown as a possible parent melt to La Soufrière magmas (Melekhova et al., 2015).

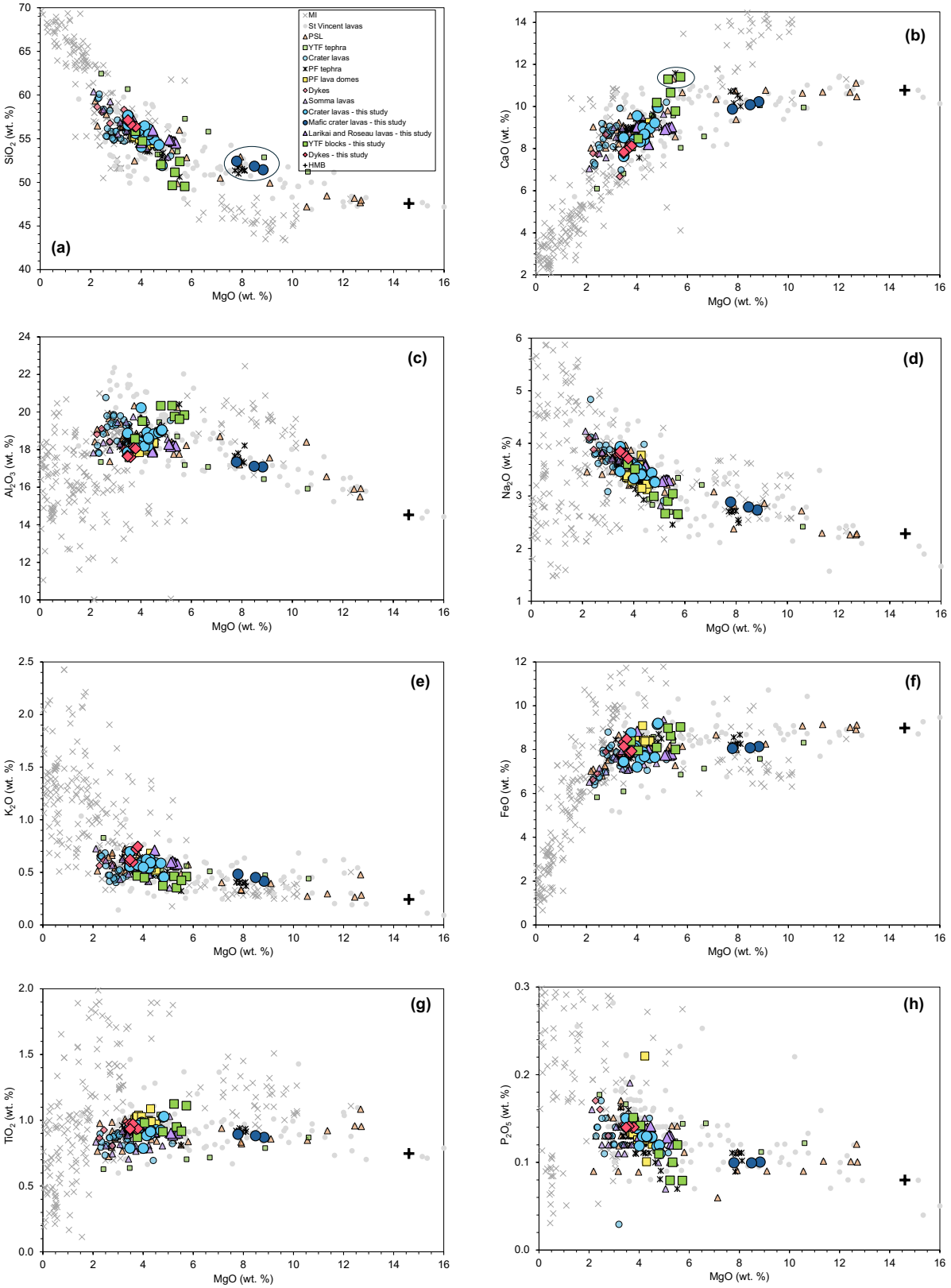

Fig 5 Major oxides versus MgO (wt. %). Magmas follow typical differentiation trends. Mafic crater lava unit (STV_LS_7, 13 and 14) circled in (a). High-Ca YTF lava blocks (STV_LS_21 and 26) circled in (b). Symbology and abbreviations as in Fig 4.

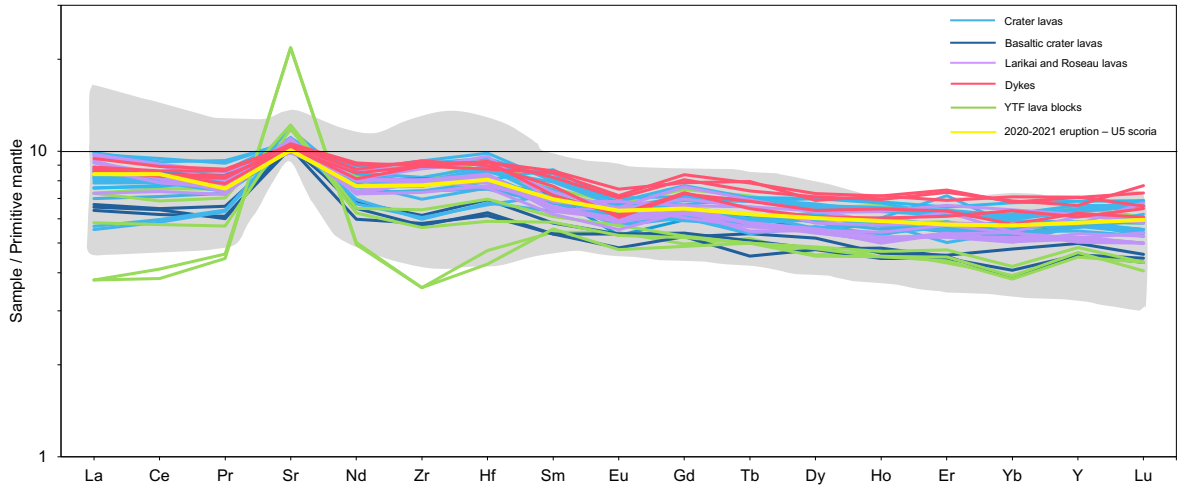

Fig 6 Spider diagram for REE elements plus Sr, Zr and Hf normalised to the primitive mantle (Sun and McDonough, 1989). Colours as in Fig 4. Grey shading represents previous St. Vincent lav and tephra data (GEOROC: Graham and Thirlwall, 1981; Dostal et al., 1983; Bardintzeff et al., 1984; Thirlwall, 1994; Heath et al., 1998; Plank, 2005; Cole et al., 2019). U5 scoria from 2020/21 eruption at La Soufrière from Holli Frey, average shown as all data near-identical (see Table 2).

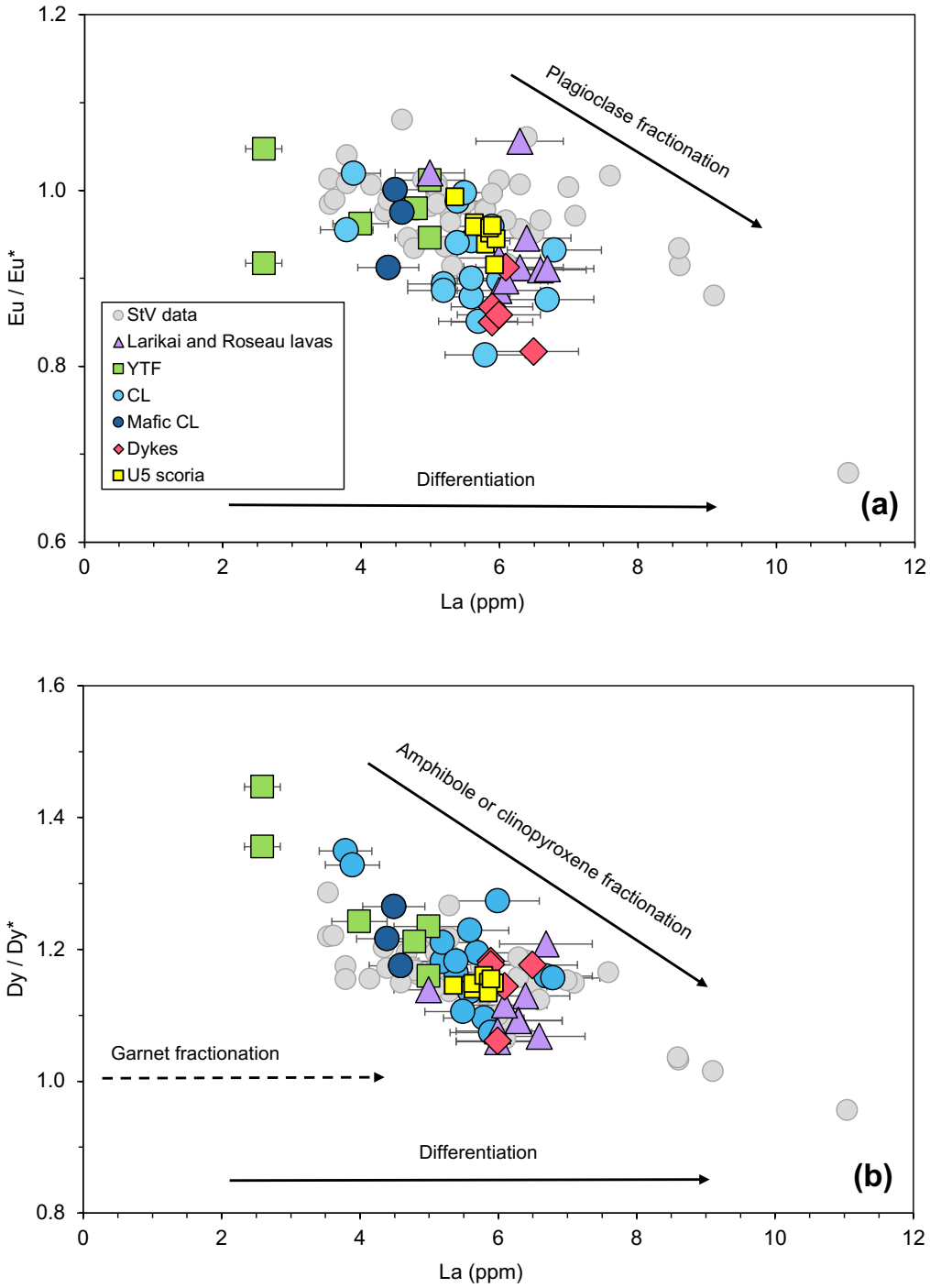

Fig 7 Lanthanum (La) versus **(a)** Eu/Eu* to determine the degree of plagioclase fractionation and **(b)** Dy/Dy* to determine the degree of clinopyroxene or amphibole fractionation experienced by magmas. Eu/Eu* calculated as interpolation between Sm and Gd (see text; Tang et al., 2021) and normalised to chondritic values of Nakamura (1974). Dy/Dy* calculated after Davidson et al. (2013).

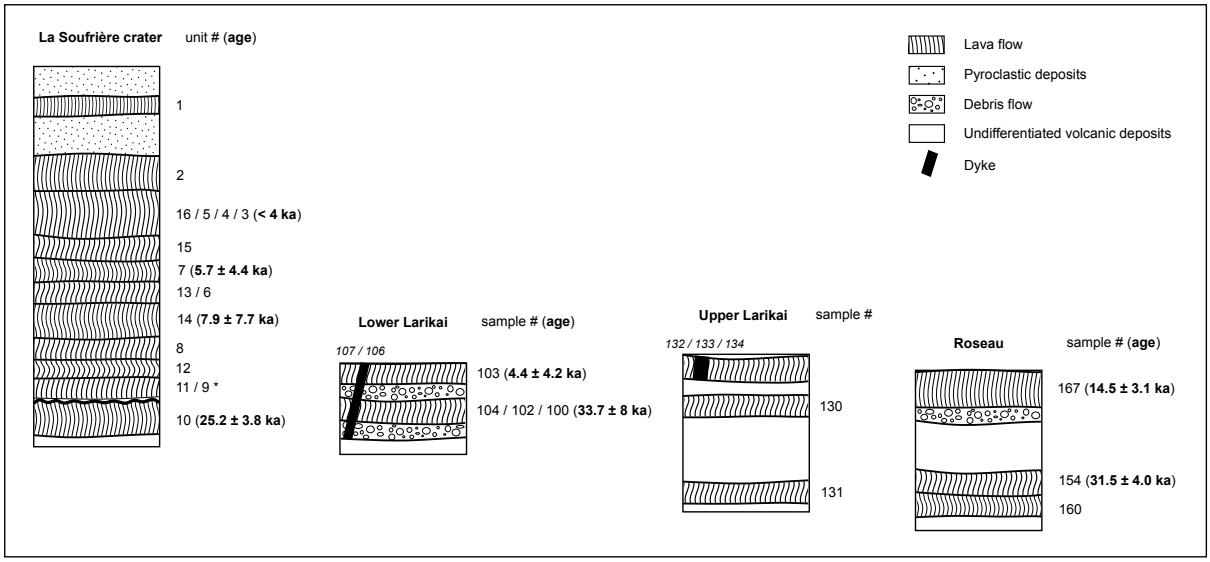

Fig 8 Stratigraphic log for the current La Soufrière crater, lower Larikai, upper Larikai and Roseau valley for samples collected. Samples shown in relative age order with known ages labelled (bold). Unit number used for the crater stratigraphic log and sample number (e.g. STV_LS_100) for all other locations. Asterix indicates mafic crater lava unit (~ 8 wt. % MgO). Dyke sample numbers in italic. Observed pyroclastic and debris flow units shown.

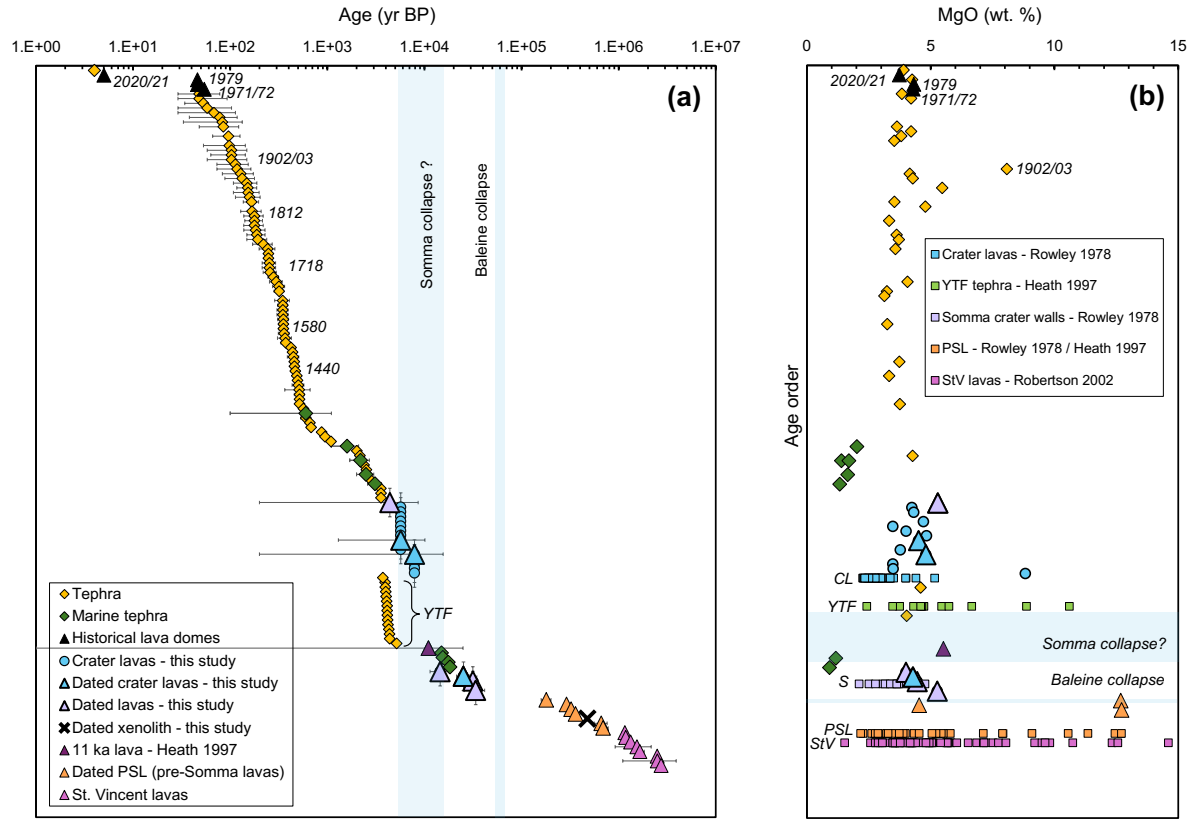

Fig 9 (a) Age (yr BP) on a log-scale versus stratigraphic position. All dates are reported in Table 4, with historical eruptions labelled. Stratigraphic relations place the crater lavas above the YTF (Sigurdsson, 1981), within error of their $^{40}Ar/^{39}Ar$ ages. The date of the Somma collapse is unknown but is tentatively linked to the YTF eruption. The dated xenolith (VSG-2) sits with the pre-Somma lavas. **(b)** MgO (wt. %) versus stratigraphic position to show compositional variation over time. Whole-rock compositions of dated lavas and tephra (containing radiocarbon dated charcoal). Note marine tephra are glass not whole-rock. Symbols as in (a). Compositions of units not dated but their relative position known are shown as squares with their colour and label correlating to volcanic period. Abbreviations include CL – crater lavas; YTF – yellow tuff formation; S – Somma lavas; PSL – pre-Somma lavas; StV – St. Vincent lavas from older volcanic centres.

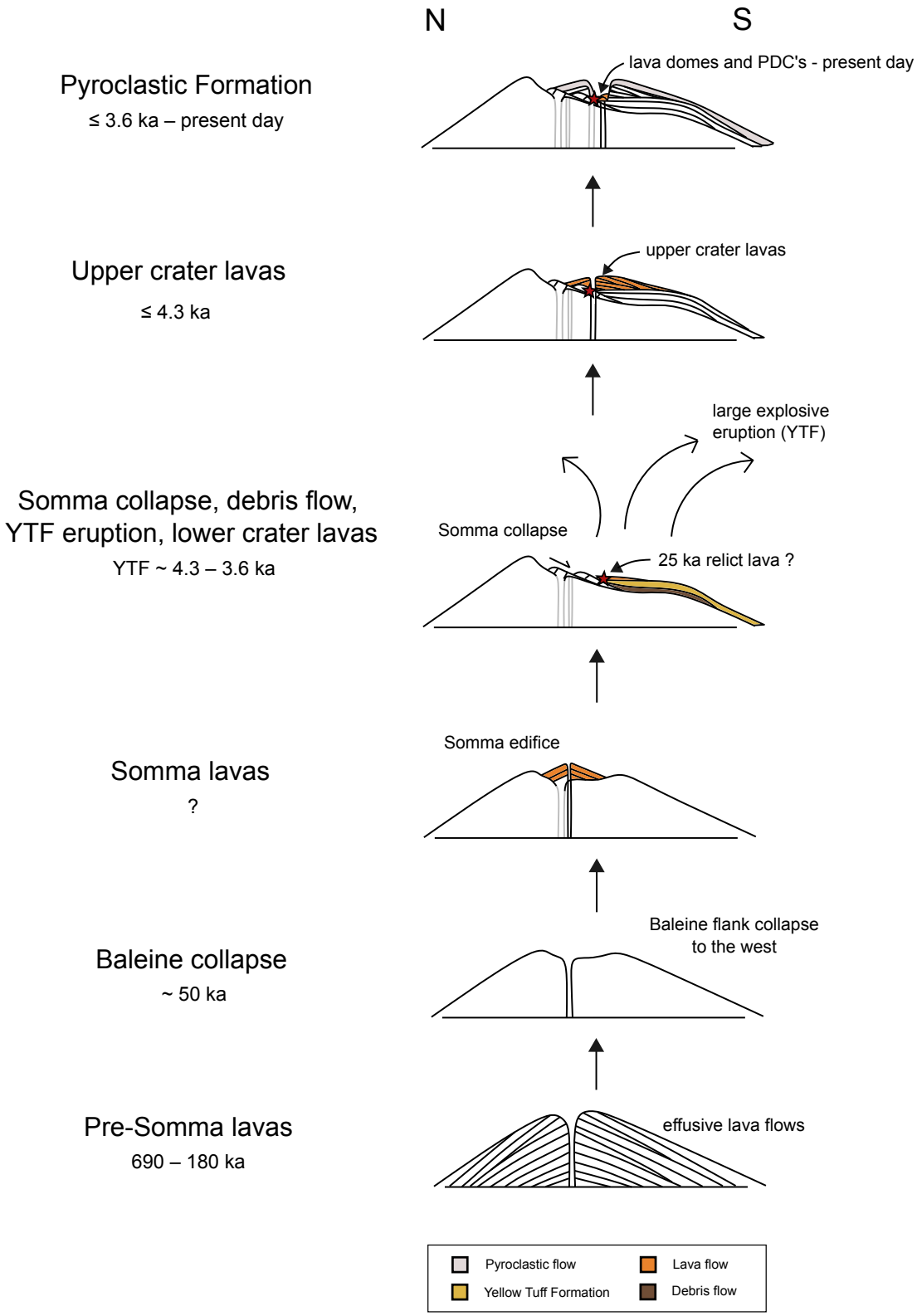

Fig 10 Schematic of revised eruptive history at La Soufrière. Pre-Somma lavas date back to 690 ± 90 ka (Briden et al., 1979). The Baleine collapse is estimated at 50 ka (Le Friant et al., 2009),

followed by the extrusion of the Somma lavas. Collapse of the Somma edifice to the south generated voluminous debris flows and parts of the crater walls likely slumped into the crater (e.g. 25.2 ± 3.8 ka crater lava depicted by a red star). The Somma collapse is also linked to the large explosive YTF eruption and possible outpourings of lava (Sigurdsson, 1981). Radiogenic dates of pyroclastic deposits constrain the YTF eruption to between 4.3 and 3.6 ka (Rowley, 1978). The crater lavas overlie the YTF deposits in the crater therefore must be younger (Sigurdsson, 1981). New $^{40}Ar/^{39}Ar$ dates have large uncertainty but give ages of 7.9 ± 7.7 ka and 5.7 ± 4.4 ka for the crater lavas. The pyroclastic formation incorporates all volcanism after the crater lavas and YTF eruption including present day eruptions. Today explosive eruptions excavate new craters and deposit thick pyroclastic units whilst effusive volcanism is restricted to within the crater.

Table 1 Whole-rock major element data

Sample #	Unit	Latitude	Longitude	SiO_2	TiO_2	Al_2O_3	FeO^T	MnO	MgO	CaO	Na_2O	K_2O	P_2O_5	Total	LOI
2023 fieldwork															
STV_LS_3	CL-1	13º20.3333' N	61º10.9004' W	54.79	0.89	18.91	7.89	0.18	4.24	9.01	3.39	0.54	0.13	99.97	-0.35
STV_LS_4a	CL-1	13º20.3334' N	61º10.9005' W	55.20	0.98	18.32	8.13	0.19	3.93	8.45	3.62	0.60	0.14	99.56	-0.20
STV_LS_4b	CL-1	13º20.3334' N	61º10.9005' W	56.03	0.98	18.28	8.09	0.19	3.91	8.45	3.63	0.59	0.14	100.29	-0.33
STV_LS_5a	CL-10	13º20.2465' N	61º10.7236' W	55.80	0.89	18.08	7.61	0.18	4.26	8.35	3.47	0.62	0.13	99.39	-0.19
STV_LS_5b	CL-10	13º20.2465' N	61º10.7236' W	56.22	0.88	18.10	7.50	0.18	4.12	8.28	3.53	0.62	0.13	99.56	-0.23
STV_LS_6	CL-7	13º20.1406' N	61º10.6068' W	54.99	0.93	18.86	7.63	0.17	4.52	8.97	3.40	0.59	0.13	100.19	-0.39
STV_LS_7	CL-9*	13º20.1175' N	61º10.5764' W	50.81	0.86	16.87	8.04	0.17	8.72	10.10	2.70	0.41	0.10	98.78	-0.26
STV_LS_8	CL-2	13º20.0397' N	61º10.49' W	55.49	0.92	18.55	7.73	0.18	4.32	8.67	3.42	0.59	0.13	100.00	-0.36
STV_LS_10	CL-2	13º20.0397' N	61º10.49' W	55.26	0.91	18.54	7.65	0.18	4.28	8.65	3.39	0.59	0.13	99.58	-0.39
STV_LS_11	CL-4	13º20.2497' N	61º10.62' W	54.63	0.93	19.04	7.69	0.17	4.74	9.28	3.46	0.59	0.12	100.65	-0.29
STV_LS_13	CL-9*	13º19.9089' N	61º10.5567' W	51.69	0.88	17.06	8.05	0.17	8.46	10.05	2.78	0.45	0.10	99.69	-0.28
STV_LS_14	CL-11*	13º19.8725' N	61º10.5830' W	52.18	0.89	17.26	8.02	0.17	7.75	9.83	2.87	0.48	0.10	99.55	-0.18
STV_LS_15	CL-12	13º19.8725' N	61º10.5830' W	55.99	0.78	18.68	7.35	0.19	3.44	8.43	3.43	0.55	0.14	98.98	-0.32
STV_LS_16	CL-5	13º19.8725' N	61º10.5830' W	57.34	0.95	17.76	7.43	0.18	3.47	7.60	3.88	0.69	0.15	99.45	-0.33
STV_LS_17	CL-5	13º19.8596' N	61º10.6014' W	57.25	0.94	17.74	7.40	0.18	3.45	7.57	3.91	0.69	0.15	99.28	-0.36
STV_LS_45	CL-13	13º19.7451' N	61º10.7844' W	55.57	0.96	18.09	8.76	0.21	3.77	8.21	3.65	0.57	0.15	99.94	-0.10
STV_LS_46	CL-14	13º19.7120' N	61º10.9211' W	51.74	1.02	18.92	9.10	0.20	4.78	9.91	3.26	0.45	0.12	99.50	-0.41
STV_LS_47	CL-15	13º19.7120' N	61º10.9211' W	51.45	1.02	18.87	9.11	0.20	4.79	9.86	3.23	0.45	0.11	99.09	-0.40
STV_LS_48	CL-16	13º19.6909' N	61º10.9311' W	54.23	0.79	20.29	7.23	0.17	4.02	9.59	3.34	0.55	0.12	100.33	-0.33
STV_LS_18	Dome			55.27	0.98	18.34	8.09	0.19	3.87	8.46	3.59	0.60	0.14	99.53	-0.36
STV_LS_20	YTF	13º13.7491' N	61º07.4935' W	50.62	0.94	19.56	8.54	0.17	5.28	10.55	2.87	0.35	0.10	98.98	0.02
STV_LS_21	YTF	13º14.1291' N	61º07.1822' W	49.44	1.12	20.25	8.94	0.16	5.21	11.25	2.65	0.46	0.08	99.56	0.15
STV_LS_22	YTF	13º14.1291' N	61º07.1822' W	55.15	0.86	18.34	8.28	0.20	3.72	8.00	3.56	0.46	0.15	98.72	0.31

STV_LS_24	YTF	13º14.1291' N	61º07.1822' W	53.62	0.96	19.12	7.80	0.18	3.97	8.30	3.44	0.44	0.14	97.97	0.65
STV_LS_25	YTF	13º14.1291' N	61º07.1822' W	51.83	0.91	20.25	8.06	0.18	4.77	10.15	2.98	0.37	0.11	99.61	-0.21
STV_LS_26	YTF	13º14.1291' N	61º07.1822' W	49.49	1.11	19.82	9.02	0.16	5.72	11.40	2.65	0.46	0.08	99.91	-0.25
STV_LS_27	YTF	13º18.2537' N	61º07.7505' W	52.03	0.91	19.48	7.95	0.17	5.49	9.71	3.02	0.42	0.12	99.30	0.31
2024 fieldwork															
STV_LS_100	LL lava	13°20.1612' N	61°12.6243' W	54.40	0.91	18.14	7.72	0.17	5.24	8.93	3.29	0.59	0.13	99.52	-0.16
STV_LS_102	LL lava	13°20.1735' N	61°12.5384' W	53.79	0.89	17.90	7.65	0.17	5.25	8.82	3.25	0.57	0.12	98.41	-0.21
STV_LS_103	LL lava	13°20.1562' N	61°12.5178' W	53.46	0.88	17.82	7.57	0.17	5.17	8.81	3.23	0.57	0.12	97.80	-0.07
STV_LS_104	LL lava	13°20.1464' N	61°12.4771' W	53.66	0.89	17.92	7.68	0.17	5.29	8.90	3.24	0.57	0.12	98.44	-0.33
STV_LS_130	UL lava	13°20.2040' N	61°11.5197' W	54.27	0.88	18.00	7.69	0.17	5.13	8.90	3.27	0.60	0.13	99.04	0.10
STV_LS_131	UL lava	13°20.3032' N	61°11.7534' W	55.32	0.91	18.43	7.80	0.18	5.15	8.98	3.30	0.60	0.13	100.80	-0.10
STV_LS_154	Roseau lava	13°19.3280' N	61°13.0440' W	55.34	0.90	17.80	7.94	0.18	4.42	8.15	3.57	0.70	0.14	99.14	-0.21
STV_LS_160	Roseau lava	13°19.3144' N	61°12.9554' W	55.12	0.90	17.61	7.87	0.18	4.39	8.07	3.51	0.70	0.14	98.49	-0.27
STV_LS_167	Roseau lava	13°19.2466' N	61°12.1695' W	54.21	0.97	18.22	8.78	0.21	3.98	8.97	3.40	0.50	0.13	99.37	-0.42
STV_LS_106	LL dyke - core	13°20.1464' N	61°12.4771' W	56.29	0.93	18.05	7.86	0.18	3.71	8.12	3.74	0.72	0.14	99.74	-0.19
STV_LS_107	LL dyke - edge	13°20.1464' N	61°12.4771' W	55.96	0.93	17.92	7.87	0.19	3.76	8.07	3.68	0.74	0.14	99.26	-0.02
STV_LS_132	UL dyke	13°20.3174' N	61°11.6433' W	56.84	0.97	17.64	8.31	0.21	3.46	7.76	3.79	0.60	0.14	99.72	-0.46
STV_LS_133	UL dyke	13°20.3174' N	61°11.6433' W	55.85	0.96	17.34	8.36	0.21	3.54	7.80	3.76	0.59	0.14	98.55	-0.39
STV_LS_134	UL dyke	13°20.3174' N	61°11.6433' W	56.87	0.93	17.56	8.11	0.21	3.46	7.80	3.83	0.62	0.14	99.53	-0.40

Latitude and longitude data in decimal degrees minutes

Abbreviations include CL - crater lava; YTF - yellow tuff formation; LL - lower Larikai; UL - upper Larikai

* Mafic crater lava units

Table 2 Trace element data and ratios

Sample #	**Unit**	Cs	Rb	Ba	Th	U	Nb	Ta	La	Ce	Pr	Sr	Nd	Zr	Hf	Sm	Eu	Gd	Tb	Dy	Ho
		ppm	ppm	ppm	ppm	ppm	ppm	ppm	ppm	ppm	ppm	ppm	ppm	ppm	ppm	ppm	ppm	ppm	ppm	ppm	ppm
2023 fieldwork																					
STV_LS_3	CL-1	0.17	11.5	121.5	1.12	0.58	2.62		5.4	13.6	2.07	228	10.1	83	2.39	2.67	1.01	3.7	0.62	4.27	0.86
STV_LS_4a	CL-1	0.56	14.3	128	1.14	0.6	2.95	0.8	6	14.6	2.29	225	11.4	87	2.67	3.52	1.11	4.1	0.74	5.15	1.11
STV_LS_4b	CL-1	0.52	13.8	128.5	1.2	0.61	3.06	0.2	5.7	15	2.39	230	11.5	92	2.75	3.74	1.1	4.22	0.74	4.82	1.06
STV_LS_5a	CL-10	0.18	14.4	133.5	1.17	0.6	2.8	1.3	5.8	15	2.3	230	10.8	91	2.46	3.19	0.89	3.55	0.66	4.05	0.95
STV_LS_5b	CL-10	0.15	13.7	132.5	1.2	0.64	2.71	0.2	5.9	14.7	2.2	226	10.4	89	2.71	3.08	1.08	3.89	0.67	4.12	0.99
STV_LS_6	CL-7	0.19	12.9	128	1.19	0.64	3.14	0.2	5.6	14.4	2.21	233	10.3	86	2.65	3.32	1.06	3.6	0.58	4.17	0.88
STV_LS_7	CL-9*	0.19	6.2	93.4	1.08	0.44	2.17	0.7	4.5	11.4	1.66	227	8.8	64	1.94	2.38	0.9	3.21	0.55	3.53	0.79
STV_LS_8	CL-2	0.21	13.3	129	1.18	0.58	2.91	0.4	5.6	14.3	2.13	233	10.9	86	2.57	3.03	0.97	3.8	0.64	4.37	0.99
STV_LS_10	CL-2	0.23	14	126	1.14	0.57	2.86	0.1	5.6	13.9	2.22	224	10.4	87	2.45	3.14	0.99	3.64	0.63	4.54	0.93
STV_LS_11	CL-4	0.15	13.4	122	1.15	0.59	3	0.4	5.5	14.2	2.1	233	9.9	83	2.45	2.91	1.04	3.53	0.62	4.11	0.95
STV_LS_13	CL-9*	0.3	10.7	94	0.88	0.38	2.13		4.4	11	1.69	216	8.1	65	1.9	2.38	0.81	3.13	0.49	3.51	0.73
STV_LS_14	CL-11*	0.37	11.2	102	0.94	0.47	2.18	0.3	4.6	11.5	1.82	217	9.2	69	2.14	2.58	0.9	3.12	0.58	3.83	0.76
STV_LS_15	CL-12	0.33	12.5	121.5	0.9	0.54	2.68	0.1	5.2	13.6	2.21	231	10.3	88	2.47	3.02	0.96	3.61	0.63	4.59	0.94
STV_LS_16	CL-5	0.22	15.2	148	1.4	0.67	3.3	0.4	6.7	16.8	2.52	228	11.8	104	3.04	3.54	1.15	4.6	0.76	4.9	1.07
STV_LS_17	CL-5	0.16	14.7	146	1.41	0.71	3.04	0.3	6.8	16.4	2.57	225	12.1	102	2.93	3.58	1.18	4.23	0.75	4.95	1.04
STV_LS_45	CL-13	0.43	12.3	112	0.83	0.47	2.53	0	5.2	13.7	2.27	225	11.5	88	2.49	3.86	1.13	3.98	0.76	5.16	1.12
STV_LS_46	CL-14	0.32	8	84.1	0.57	0.37	2.32		3.8	10.4	1.75	229	9.1	68	2.06	3.19	1.05	3.58	0.63	4.39	0.98
STV_LS_47	CL-15	0.31	8.3	86.8	0.54	0.36	2.23	0.4	3.9	10.6	1.77	233	9.4	67	2.09	2.82	1.1	3.9	0.65	4.62	0.94
STV_LS_48	CL-16	0.19	10.2	110.5	1.06	0.52	2.64	0.2	5.4	14	2.04	248	10.6	78	2.34	3.08	1.03	3.68	0.58	4.16	0.87
STV_LS_18	Dome	0.52	14.9	128	1.17	0.58	3	0.5	5.7	14.6	2.29	226	11.2	89	2.9	3.35	1.13	4.46	0.77	4.8	1.09
STV_LS_20	YTF	0.1	4	91	0.23	0.18	1.08	0	2.6	6.8	1.23	460	6.8	40	1.46	2.41	0.91	2.96	0.56	3.37	0.77
STV_LS_21	YTF	0.13	7.5	78.5	0.65	0.34	2.5	0.2	5	13.4	2.07	218	10.6	87	2.67	3.25	1.1	3.93	0.64	4.49	0.95
STV_LS_24	YTF	0.1	9.6	96.9	0.7	0.41	2.34	0.4	4.8	12.6	2.01	216	9.9	83	2.32	2.99	1.08	3.84	0.67	4.31	0.91
STV_LS_25	YTF	0.13	6.9	77.6	0.56	0.35	1.94	0.3	4	10.2	1.57	250	8.5	63	1.82	2.6	0.89	3.11	0.54	3.58	0.77
STV_LS_26	YTF	0.08	4.1	90.9	0.24	0.15	1.12	0.1	2.6	7.3	1.27	459	6.7	40	1.32	2.47	0.8	2.91	0.54	3.53	0.74
STV_LS_27	YTF	0.21	9.5	96	0.81	0.45	2.87	0.3	5	12.2	1.94	257	8.8	72	2.15	2.71	0.96	3.14	0.54	3.34	0.74

Table 2 Continued

Sample #	Unit	Cs	Rb	Ba	Th	U	Nb	Ta	La	Ce	Pr	Sr	Nd	Zr	Hf	Sm	Eu	Gd	Tb	Dy	Ho
		ppm	ppm	ppm	ppm	ppm	ppm	ppm	ppm	ppm	ppm	ppm	ppm	ppm	ppm	ppm	ppm	ppm	ppm	ppm	ppm
2024 fieldwork																					
STV_LS_100	LL lava	0.52	13.9	129.5	1.28	0.66	2.92	0.2	6	14.7	2.02	221	10	90	2.34	2.76	0.93	3.77	0.59	4.05	0.89
STV_LS_102	LL lava	0.2	13.1	127	1.2	0.62	2.75	0.1	6.3	15	2.15	226	11	90	2.6	2.91	1.01	3.98	0.62	3.97	0.84
STV_LS_103	LL lava	0.16	13	122	1.16	0.59	2.61	0.1	6	14	2.11	222	9.8	89	2.43	2.93	0.99	3.71	0.63	4	0.83
STV_LS_104	LL lava	0.14	13.1	119.5	1.21	0.67	2.9	0.1	6.1	14	2.09	232	9.8	89	2.53	2.92	0.98	3.86	0.59	4.06	0.82
STV_LS_130	UL lava	0.53	14.6	127.5	1.26	0.6	2.58	0.1	6.4	14.4	2.11	229	10.8	90	2.56	2.82	1.01	3.82	0.63	4.11	0.86
STV_LS_131	UL lava	0.53	14.3	124	1.28	0.63	2.86	0.1	6.3	14.4	2.09	225	10.4	89	2.55	2.84	1.1	3.61	0.61	4.06	0.86
STV_LS_154	Roseau lava	0.27	13.8	148	1.27	0.69	3.01	0.1	6.6	15.9	2.21	209	11.8	99	2.97	3.03	1.1	4.56	0.75	4.64	1.04
STV_LS_160	Roseau lava	0.23	14.4	145.5	1.27	0.72	3.21	0.6	6.7	16.1	2.36	208	11	98	2.84	3.26	1.09	4.15	0.71	4.69	0.96
STV_LS_167	Roseau lava	0.12	9.1	105.5	0.7	0.39	2.28	0.1	5	13.1	1.99	229	9.8	82	2.38	3.04	1.15	3.95	0.71	4.29	0.94
STV_LS_106	LL dyke - core	0.43	16.3	133.5	1.19	0.62	2.55	0.1	6	14.9	2.29	214	11.5	100	2.85	3.18	1.04	4.36	0.7	4.49	0.99
STV_LS_107	LL dyke - edge	0.63	16	141.5	1.22	0.65	2.76	0.1	6.5	15.8	2.41	219	11.8	104	2.77	3.41	1.02	4.32	0.74	4.72	1.06
STV_LS_132	UL dyke	0.2	11.4	133.5	0.96	0.61	2.59	0.1	6.1	15.3	2.38	221	12.2	102	2.84	3.83	1.26	4.7	0.86	5.08	1.17
STV_LS_133	UL dyke	0.17	11.6	128	1.01	0.58	2.4	0.1	5.9	14.7	2.25	223	12.4	100	2.7	3.77	1.2	4.99	0.85	5.35	1.17
STV_LS_134	UL dyke	0.14	11.8	131.5	1.07	0.56	2.39	0.1	5.9	14.8	2.16	217	11	100	2.86	3.64	1.18	4.8	0.8	5.22	1.14
2020-2021 eruption																					
411-SVG-1*	U5 scoria	0.50	12.1	109.9	0.95	0.51	2.69	0.2	5.4	13.8	1.95	217	9.6	81	2.31	2.87	1.04	3.58	0.63	4.13	0.90
411-SVG-2*	U5 scoria	0.53	12.6	114.3	1.01	0.55	2.83	0.2	5.6	14.6	2.03	214	10.1	85	2.46	3.01	1.05	3.72	0.65	4.30	0.94
411-SVG-7*	U5 scoria	0.53	12.4	112.8	0.99	0.53	2.74	0.2	5.6	14.5	2.03	209	10.3	84	2.44	3.04	1.07	3.87	0.67	4.45	0.97
411-SVG-8*	U5 scoria	0.55	13.2	119.7	1.05	0.57	2.90	0.2	5.8	15.0	2.09	212	10.5	89	2.52	3.11	1.06	3.89	0.67	4.45	0.96
411-SVG-11a*	U5 scoria	0.58	13.1	119.7	1.06	0.57	2.95	0.2	5.9	15.3	2.14	213	10.7	89	2.53	3.19	1.06	3.98	0.69	4.55	1.00
411-SVG-11B*	U5 scoria	0.57	13.3	119.6	1.06	0.57	2.95	0.2	5.9	15.2	2.12	216	10.6	89	2.54	3.15	1.09	3.93	0.68	4.55	0.99
411-SVG-12A*	U5 scoria	0.58	13.5	119.7	1.19	0.59	2.93	0.2	6.0	15.3	2.14	210	10.6	88	2.54	3.18	1.09	3.96	0.69	4.59	0.99
411-SVG-12B-2*	U5 scoria	0.59	13.3	119.7	1.20	0.60	2.88	0.2	5.9	15.2	2.12	212	10.5	87	2.51	3.14	1.09	3.89	0.68	4.49	0.98
411-SVG-12B-2*	U5 scoria	0.59	13.3	120.5	1.21	0.60	2.91	0.2	5.9	15.3	2.13	211	10.6	88	2.54	3.16	1.10	3.92	0.68	4.55	0.99

Table 2 Continued

Sample #	Unit	Er	Yb	Y	Lu	Tm	Sc	V	Cr	Ga	W	Th/ Nb	La/ Sm	Ba/ Th	U/ Th	Ce/ Yb	Th/ Yb	Dy/ Yb	Ba/ La	Dy / Dy*	Eu / Eu*
		ppm	ppm	ppm	ppm	ppm	ppm	ppm	ppm	ppm	ppm										
2023 fieldwork																					
STV_LS_3	CL-1	2.73	2.65	25.2	0.46	0.42	35.1	286	12	20	0.8	0.43	2.02	108	0.52	5.13	0.42	1.61	22.50	1.17	0.99
STV_LS_4a	CL-1	2.97	2.95	28.8	0.49	0.46	35.4	273	17	19.7	0.9	0.39	1.70	112	0.53	4.95	0.39	1.75	21.33	1.27	0.90
STV_LS_4b	CL-1	2.97	2.99	29.5	0.49	0.48	35.8	265	18	20	0.7	0.39	1.52	107	0.51	5.02	0.40	1.61	22.54	1.19	0.85
STV_LS_5a	CL-10	2.61	2.62	26.3	0.4	0.38	34.2	270	51	18.9	0.7	0.42	1.82	114	0.51	5.73	0.45	1.55	23.02	1.10	0.81
STV_LS_5b	CL-10	2.74	2.75	26.6	0.39	0.45	35.1	258	41	19.1	0.8	0.44	1.92	110	0.53	5.35	0.44	1.50	22.46	1.07	0.96
STV_LS_6	CL-7	2.71	2.6	26.1	0.41	0.4	35	277	48	19.1	2.5	0.38	1.69	108	0.54	5.54	0.46	1.60	22.86	1.14	0.94
STV_LS_7	CL-9*	2.17	1.9	20.7	0.32	0.34	46.8	307	409	17.1	0.7	0.50	1.89	86	0.41	6.00	0.57	1.86	20.76	1.27	1.00
STV_LS_8	CL-2	3.43	2.81	25.7	0.46	0.45	35.2	277	36	19.2	1.1	0.41	1.85	109	0.49	5.09	0.42	1.56	23.04	1.14	0.88
STV_LS_10	CL-2	2.63	2.65	25.6	0.44	0.43	34.5	277	32	18.8	0.7	0.40	1.78	111	0.50	5.25	0.43	1.71	22.50	1.23	0.90
STV_LS_11	CL-4	2.41	2.69	24.9	0.39	0.4	36.8	284	51	18.8	0.9	0.38	1.89	106	0.51	5.28	0.43	1.53	22.18	1.11	1.00
STV_LS_13	CL-9*	2.14	2.01	20.8	0.33	0.34	47.6	303	364	16.4	0.7	0.41	1.85	107	0.43	5.47	0.44	1.75	21.36	1.22	0.91
STV_LS_14	CL-11*	2.19	2.36	22.7	0.34	0.31	46.5	302	320	17.9	0.8	0.43	1.78	109	0.50	4.87	0.40	1.62	22.17	1.18	0.98
STV_LS_15	CL-12	2.67	2.92	26.7	0.43	0.43	30.8	219	9	19.1	0.8	0.34	1.72	135	0.60	4.66	0.31	1.57	23.37	1.18	0.89
STV_LS_16	CL-5	3.08	3.03	29.4	0.51	0.48	33.6	262	22	18.7	0.8	0.42	1.89	106	0.48	5.54	0.46	1.62	22.09	1.16	0.88
STV_LS_17	CL-5	2.96	3.07	30.2	0.49	0.47	34.1	260	21	18.8	0.7	0.46	1.90	104	0.50	5.34	0.46	1.61	21.47	1.16	0.93
STV_LS_45	CL-13	3.15	3.34	31.2	0.51	0.47	31.8	255	5	19.1	<0.5	0.33	1.35	135	0.57	4.10	0.25	1.54	21.54	1.21	0.89
STV_LS_46	CL-14	2.73	2.51	26.6	0.41	0.42	43.5	348	12	19.4	0.7	0.25	1.19	148	0.65	4.14	0.23	1.75	22.13	1.35	0.96
STV_LS_47	CL-15	2.66	2.74	26.3	0.41	0.44	40.7	350	11	19.7	0.7	0.24	1.38	161	0.67	3.87	0.20	1.69	22.26	1.33	1.02
STV_LS_48	CL-16	2.82	2.5	25.8	0.4	0.42	28.9	216	24	18.3	0.7	0.40	1.75	104	0.49	5.60	0.42	1.66	20.46	1.18	0.94
STV_LS_18	Dome	3	3.07	29.8	0.45	0.47	37.2	274	18	19.1	1	0.39	1.70	109	0.50	4.76	0.38	1.56	22.46	1.17	0.90
STV_LS_20	YTF	2.07	1.93	20.8	0.32	0.29	47.6	433	37	17.5	0.7	0.21	1.08	396	0.78	3.52	0.12	1.75	35.00	1.36	1.05
STV_LS_21	YTF	2.82	2.69	26.7	0.43	0.45	24.5	192	30	20.8	0.7	0.26	1.54	121	0.52	4.98	0.24	1.67	15.70	1.23	0.95
STV_LS_24	YTF	2.71	2.64	25.8	0.45	0.4	30.6	240	40	19.2	0.8	0.30	1.61	138	0.59	4.77	0.27	1.63	20.19	1.21	0.98
STV_LS_25	YTF	2.28	2.07	22	0.32	0.35	35.1	292	43	19	0.6	0.29	1.54	139	0.63	4.93	0.27	1.73	19.40	1.24	0.96
STV_LS_26	YTF	2.1	1.88	20.5	0.32	0.34	49.5	448	44	17	0.7	0.21	1.05	379	0.63	3.88	0.13	1.88	34.96	1.45	0.92
STV_LS_27	YTF	2.16	1.92	21.2	0.3	0.31	31.5	259	133	19.3	0.8	0.28	1.85	119	0.56	6.35	0.42	1.74	19.20	1.16	1.01

Table 2 Continued

Sample #	Unit	Er	Yb	Y	Lu	Tm	Sc	V	Cr	Ga	W	Th/ Nb	La/ Sm	Ba/ Th	U/ Th	Ce/ Yb	Th/ Yb	Dy/ Yb	Ba/ La	Dy / Dy*	Eu / Eu*
		ppm	ppm	ppm	ppm	ppm	ppm	ppm	ppm	ppm	ppm										
2024 fieldwork																					
STV_LS_100	LL lava	2.74	2.66	23.6	0.4	0.35	34.9	274	128	21.5	0.9	0.44	2.17	101	0.52	5.53	0.48	1.52	21.58	1.08	0.89
STV_LS_102	LL lava	2.59	2.49	23.4	0.37	0.37	35.7	268	137	20.5	0.5	0.44	2.16	106	0.52	6.02	0.48	1.59	20.16	1.09	0.91
STV_LS_103	LL lava	2.57	2.67	22.9	0.37	0.4	33.6	259	134	21.4	0.9	0.44	2.05	105	0.51	5.24	0.43	1.50	20.33	1.06	0.92
STV_LS_104	LL lava	2.57	2.52	23.8	0.37	0.4	36.1	270	136	20.3	0.6	0.42	2.09	99	0.55	5.56	0.48	1.61	19.59	1.12	0.90
STV_LS_130	UL lava	2.51	2.48	24.4	0.39	0.37	36	263	116	20.8	0.5	0.49	2.27	101	0.48	5.81	0.51	1.66	19.92	1.13	0.95
STV_LS_131	UL lava	2.52	2.57	23.8	0.37	0.38	34.1	256	117	20.8	0.6	0.45	2.22	97	0.49	5.60	0.50	1.58	19.68	1.09	1.06
STV_LS_154	Roseau lava	3.19	3.17	28.2	0.43	0.51	37	247	49	21.8	<0.5	0.42	2.18	117	0.54	5.02	0.40	1.46	22.42	1.07	0.91
STV_LS_160	Roseau lava	3.03	2.68	27.8	0.45	0.48	37.1	248	58	21.5	0.6	0.40	2.06	115	0.57	6.01	0.47	1.75	21.72	1.21	0.91
STV_LS_167	Roseau lava	2.8	2.83	26.3	0.5	0.42	36.1	286	17	23.1	0.6	0.31	1.64	151	0.56	4.63	0.25	1.52	21.10	1.14	1.02
STV_LS_106	LL dyke - core	2.94	3.15	27.7	0.48	0.46	33.1	250	20	22	0.5	0.47	1.89	112	0.52	4.73	0.38	1.43	22.25	1.06	0.86
STV_LS_107	LL dyke - edge	3.06	2.84	28.5	0.45	0.49	34.8	257	18	21.7	0.5	0.44	1.91	116	0.53	5.56	0.43	1.66	21.77	1.18	0.82
STV_LS_132	UL dyke	3.58	3.36	32.1	0.54	0.55	33.5	243	8	23.3	0.7	0.37	1.59	139	0.64	4.55	0.29	1.51	21.89	1.14	0.91
STV_LS_133	UL dyke	3.31	3.49	32.2	0.49	0.5	35.5	245	7	22.8	<0.5	0.42	1.56	127	0.57	4.21	0.29	1.53	21.69	1.18	0.85
STV_LS_134	UL dyke	3.52	3.39	30.2	0.57	0.57	31.7	223	8	21.9	0.6	0.45	1.62	123	0.52	4.37	0.32	1.54	22.29	1.18	0.87
2020-2021 eruption																					
411-SVG-1*	U5 scoria	2.56	2.60	24.7	0.41	0.39	29.8	233	26	17.9		0.35	1.87	116	0.54	5.30	0.36	1.59	20.49	1.14	0.99
411-SVG-2*	U5 scoria	2.69	2.73	26.0	0.43	0.41	29.3	227	23	17.9		0.36	1.88	113	0.54	5.35	0.37	1.58	20.26	1.14	0.96
411-SVG-7*	U5 scoria	2.75	2.83	26.1	0.44	0.42	33.5	236	20	18.3		0.36	1.85	114	0.54	5.12	0.35	1.57	20.00	1.15	0.96
411-SVG-8*	U5 scoria	2.77	2.77	26.9	0.44	0.42	29.0	237	21	17.9		0.36	1.87	114	0.54	5.43	0.38	1.61	20.62	1.16	0.94
411-SVG-11a*	U5 scoria	2.82	2.87	27.0	0.45	0.44	29.7	246	22	18.1		0.36	1.86	113	0.54	5.34	0.37	1.58	20.18	1.15	0.92
411-SVG-11B*	U5 scoria	2.81	2.88	27.2	0.45	0.43	30.3	254	22	18.5		0.36	1.86	112	0.53	5.26	0.37	1.58	20.38	1.15	0.95
411-SVG-12A*	U5 scoria	2.83	2.90	27.0	0.45	0.44	31.0	258	25	18.2		0.41	1.88	100	0.50	5.28	0.41	1.58	20.09	1.15	0.94
411-SVG-12B-2*	U5 scoria	2.80	2.88	26.8	0.45	0.42	31.1	256	25	17.9		0.42	1.87	100	0.50	5.26	0.41	1.56	20.40	1.13	0.96
411-SVG-12B-2*	U5 scoria	2.81	2.85	27.2	0.45	0.43	30.8	259	25	18.2		0.41	1.87	100	0.50	5.37	0.42	1.59	20.40	1.15	0.96

* Data from Holli Frey analysed via dissolution on an Agilent 8900 ICP-MS at the Department of Geosciences, Union College, New York
No data for STV_LS_20 due to contamination.

Table 3 New $^{40}Ar/^{39}Ar$ data for La Soufrière

				Isochron		Plateau				
Sample #	Location	$^{40}Ar/^{36}Ar_i$ ± 2s		Age (ka) ± 2s		Age (ka) ± 2s		N	^{39}Ar %	MSWD
STV-LS-6	Crater	296.5	± 3.7	16.4	± 19.8	5.7	± 4.4	11/16	90.5	0.92
STV-LS-46	Crater	298.2	± 1.3	12.3	± 18.9	7.9	± 7.7	13/14	98.3	0.46
STV-LS-5a	Crater	299.2	± 1.7	21.6	± 11.0	25.2	± 3.8	16/17	99.7	0.59
STV-LS-103	Lower Larikai	298.4	± 2.2	5.4	± 13.7	4.4	± 4.2	12/18	91.4	0.56
STV-LS-100	Lower Larikai	299.3	± 0.9	22.6	± 15.5	33.7	± 8.0	15/18	95.5	0.36
STV-LS-167	Roseau	298.5	± 2.3	14.7	± 7.9	14.5	± 3.1	14/18	95.0	1.03
STV-LS-154	Roseau	298.5	± 1.3	31.9	± 8.9	31.5	± 4.0	15/19	90.7	1.01
VSG-2	Jacobs well	298.6	± 0.5	474.0	± 37.6	475.6	± 28.3	13/14	99.8	0.55

Ages calculated relative to 1.1864 Ma Alder Creek sanidine standard (Jicha et al., 2016) using the decay constants of Min et al. (2000).
Atmospheric $^{40}Ar/^{36}Ar$ = 298.56 ± 0.31 (Lee et al., 2006)
N = number of incremental heating steps

Table 4 K/Ar, $^{40}Ar/^{39}Ar$, ^{14}C and foraminifera dates for St. Vincent lavas, pyroclastic deposits and marine tephra in age order.

Volcanic centre	Location	Sample #	Reference	Method	Age
Pyroclastics					
La Soufrière 1902	Dry Wallibou	C45	Cole et al., 2019.	^{14}C (yr BP)	20 ± 30
La Soufrière	Rabacca River	SVE-104	Heath 1997	^{14}C (yr BP)	20 ± 45
La Soufrière	Dry Wallibou River	SRR-3972	Robertson 1992	^{14}C (yr BP)	20 ± 4
La Soufrière	Rabacca River	SVE-102	Heath 1997	^{14}C (yr BP)	30 ± 45
La Soufrière	Dry Wallibou River	STV-123	Heath 1997	^{14}C (yr BP)	40 ± 45
La Soufrière	Dry Wallibou River	SRR-3973	Robertson 1992	^{14}C (yr BP)	45 ± 40
La Soufrière	Wallibou River	SVE-094	Heath 1997	^{14}C (yr BP)	55 ± 50
La Soufrière	Camariabou River	SVE-111	Heath 1997	^{14}C (yr BP)	70 ± 45
La Soufrière	Rabacca River	SVE-105	Heath 1997	^{14}C (yr BP)	75 ± 45
La Soufrière	Dry Wallibou River	SVE-090	Heath 1997	^{14}C (yr BP)	75 ± 40
La Soufrière	Sandy Bay	STV-112	Heath 1997	^{14}C (yr BP)	75 ± 45
La Soufrière 1812	Dry Wallibou	C4	Cole et al., 2019.	^{14}C (yr BP)	79 ± 37
La Soufrière	Dry Wallibou River	SRR-3974	Robertson 1992	^{14}C (yr BP)	80 ± 40
La Soufrière 1812 / 1718	Wallibou coast	C49	Cole et al., 2019.	^{14}C (yr BP)	90 ± 30
La Soufrière	Rabacca River	SVE-101	Heath 1997	^{14}C (yr BP)	90 ± 45
La Soufrière	Rabacca River	SVE-103	Heath 1997	^{14}C (yr BP)	100 ± 45
La Soufrière	Rabacca River	SVE-106	Heath 1997	^{14}C (yr BP)	105 ± 45
La Soufrière	Wallibou River	SVE-086	Heath 1997	^{14}C (yr BP)	120 ± 40
La Soufrière	Dry Wallibou River	SVE-097	Heath 1997	^{14}C (yr BP)	125 ± 45
La Soufrière	Wallibou River	SVE-085	Heath 1997	^{14}C (yr BP)	130 ± 45
La Soufrière	Morne Ronde River	SRR-3967(a)	Robertson 1992	^{14}C (yr BP)	135 ± 40
La Soufrière	Morne Ronde River	SRR-3967(b)	Robertson 1992	^{14}C (yr BP)	145 ± 40
La Soufrière 1812 / 1718	Proximal SE flank	C8a	Cole et al., 2019.	^{14}C (yr BP)	146 ± 35
La Soufrière	Dry Wallibou River	SVE-089	Heath 1997	^{14}C (yr BP)	150 ± 40
La Soufrière	Owia	SVE-099	Heath 1997	^{14}C (yr BP)	155 ± 45
La Soufrière 1812 / 1718	Windward trail SE flank	C53	Cole et al., 2019.	^{14}C (yr BP)	160 ± 30
La Soufrière	Wallibou River	SVE-084	Heath 1997	^{14}C (yr BP)	160 ± 40
La Soufrière	Dry Wallibou River	STV-106	Heath 1997	^{14}C (yr BP)	165 ± 45
La Soufrière 1812 / 1718	Proximal SE flank	C10	Cole et al., 2019.	^{14}C (yr BP)	172 ± 37
La Soufrière	Rabacca Valley	37302	Rowley 1978	^{14}C (yr BP)	173 ± 50
La Soufrière	Chibarabu Point	842	Rowley 1978	^{14}C (yr BP)	200
La Soufrière	Wallibou sea-cliff	838	Rowley 1978	^{14}C (yr BP)	200
La Soufrière	Dry Wallibou	STV-366	Heath 1997	^{14}C (yr BP)	215 ± 45
La Soufrière	Wallibou sea-cliff	SRR-3960	Robertson 1992	^{14}C (yr BP)	220 ± 40
La Soufrière	Morne Ronde River	SRR-3968	Robertson 1992	^{14}C (yr BP)	220 ± 40
La Soufrière	Wallibou sea-cliff	SRR-3971	Robertson 1992	^{14}C (yr BP)	225 ± 40
La Soufrière	Morne Ronde Valley	79-56	Heath 1997	^{14}C (yr BP)	270 ± 45
La Soufrière 1560	Dry Wallibou valley	C2	Cole et al., 2019.	^{14}C (yr BP)	273 ± 35
La Soufrière	Dry Wallibou River	STV-131	Heath 1997	^{14}C (yr BP)	290 ± 45
La Soufrière	N. Wallibou Dry River	902	Rowley 1978	^{14}C (yr BP)	300 ± 60
La Soufrière 1566	Dry Wallibou	C3	Cole et al., 2019.	^{14}C (yr BP)	313 ± 35
La Soufrière	Wallibou sea-cliff	SRR-3961	Robertson 1992	^{14}C (yr BP)	315 ± 40
La Soufrière	N. Wallibou Dry River	901	Rowley 1978	^{14}C (yr BP)	320 ± 60
La Soufrière	Dry Wallibou River	SVE-095	Heath 1997	^{14}C (yr BP)	320 ± 45
La Soufrière	Windward Trail	STV-329	Heath 1997	^{14}C (yr BP)	320 ± 45
La Soufrière	Dry Wallibou River	STV-117	Heath 1997	^{14}C (yr BP)	330 ± 45
La Soufrière	Dry Wallibou River	SVE-088	Heath 1997	^{14}C (yr BP)	325 ± 45
La Soufrière	Larikai sea-cliff	SRR-3965	Robertson 1992	^{14}C (yr BP)	340 ± 40
La Soufrière 1590	SW coast	C5	Cole et al., 2019.	^{14}C (yr BP)	347 ± 35
La Soufrière 1551	Proximal SE flank	C11	Cole et al., 2019.	^{14}C (yr BP)	347 ± 35
La Soufrière	Larikai sea-cliff	SRR-3964	Robertson 1992	^{14}C (yr BP)	390 ± 40
La Soufrière	Larikai sea-cliff	870	Rowley 1978	^{14}C (yr BP)	400 ± 60
La Soufrière	Wallibou sea-cliff	SRR-3959	Robertson 1992	^{14}C (yr BP)	405 ± 40
La Soufrière	Larikai sea-cliff	SRR-3962	Robertson 1992	^{14}C (yr BP)	425 ± 40
La Soufrière	Windward Trail	STV-066	Heath 1997	^{14}C (yr BP)	440 ± 45
La Soufrière 1445	Larakai sea-cliff	C63	Cole et al., 2019.	^{14}C (yr BP)	450 ± 30
La Soufrière	Wallibou River	SVE-087	Heath 1997	^{14}C (yr BP)	465 ± 45
La Soufrière	Larikai River	37273	Rowley 1978	^{14}C (yr BP)	467 ± 150
La Soufrière	Larikai River	903	Rowley 1978	^{14}C (yr BP)	470 ± 60
La Soufrière	Windward Trail	STV-072	Heath 1997	^{14}C (yr BP)	475 ± 70
La Soufrière 1430	Larakai sea-cliff	C61	Cole et al., 2019.	^{14}C (yr BP)	480 ± 30
La Soufrière	Larikai sea-cliff	SRR-3963	Robertson 1992	^{14}C (yr BP)	485 ± 40
La Soufrière	Larikai beach	STV-370	Heath 1997	^{14}C (yr BP)	490 ± 45
La Soufrière	Roseau River	SRR-3970	Robertson 1992	^{14}C (yr BP)	535 ± 45
La Soufrière	Wallibou sea-cliff	841	Rowley 1978	^{14}C (yr BP)	555 ± 70
La Soufrière	Soufrière path (E. 650 m)	843	Rowley 1978	^{14}C (yr BP)	615 ± 60
La Soufrière	Wallibou Dry River	840	Rowley 1978	^{14}C (yr BP)	635 ± 65
La Soufrière 1157	Windward trail	C8	Cole et al., 2019.	^{14}C (yr BP)	870 ± 37
La Soufrière	Roseau River	SRR-3969	Robertson 1992	^{14}C (yr BP)	915 ± 45
La Soufrière	Soufrière path (E. 650 m)	844	Rowley 1978	^{14}C (yr BP)	1045 ± 70
La Soufrière	Mouth of Waribishy River	SVE-080	Heath 1997	^{14}C (yr BP)	1985 ± 40
La Soufrière	Waribishy River	STV-348	Heath 1997	^{14}C (yr BP)	2135 ± 40
La Soufrière	New Sandy Bay*	STV-104	Heath 1997	^{14}C (yr BP)	2360 ± 50
La Soufrière	Overland Village	781	Rowley 1978	^{14}C (yr BP)	2480 ± 70
La Soufrière	Waribishy River	778	Rowley 1978	^{14}C (yr BP)	2700 ± 90

La Soufrière	Rabacca Valley	37209	Rowley 1978	^{14}C (yr BP)	3510 ± 65
La Soufrière	Rabacca Valley	27737	Rowley 1978	^{14}C (yr BP)	3520 ± 70
La Soufrière	Dry Rabacca bed	STV-360	Heath 1997	^{14}C (yr BP)	3550 ± 45
La Soufrière	Lower Rabacca	900	Rowley 1978	^{14}C (yr BP)	3590 ± 70
La Soufrière	Dry Rabacca River	STV-084	Heath 1997	^{14}C (yr BP)	3705 ± 70
La Soufrière	Lower Rabacca	59-1	Hay 1959 / Rowley 1978	^{14}C (yr BP)	3890 ± 300
La Soufrière	Rabacca River	STV-305a	Heath 1997	^{14}C (yr BP)	3925 ± 45
La Soufrière	Rabacca	845	Rowley 1978	^{14}C (yr BP)	3960 ± 80
La Soufrière	Rabacca Gorge	766	Rowley 1978	^{14}C (yr BP)	3980 ± 80
La Soufrière	Waterloo sea-cliff	SRR-3966	Robertson 1992	^{14}C (yr BP)	4040 ± 45
La Soufrière	Rabacca	760	Rowley 1978	^{14}C (yr BP)	4080 ± 60
La Soufrière	Rabacca River	59-2	Hay 1959 / Rowley 1978	^{14}C (yr BP)	4090 ± 50
La Soufrière	Rabacca River	STV-305b	Heath 1997	^{14}C (yr BP)	4120 ± 45
La Soufrière	Sea-cliff, North Rabacca	777	Rowley 1978	^{14}C (yr BP)	4130 ± 160
La Soufrière	Rabacca Valley	846	Rowley 1978	^{14}C (yr BP)	4165 ± 70
La Soufrière	Rabacca Gorge	765	Rowley 1978	^{14}C (yr BP)	4260 ± 120
La Soufrière	Rabacca Gorge	764	Rowley 1978	^{14}C (yr BP)	4325 ± 95
La Soufrière	Rabacca Valley	761	Rowley 1978	^{14}C (yr BP)	4335 ± 95
La Soufrière	Owia*	SVE-98	Heath 1997	^{14}C (yr BP)	5140 ± 55
Marine Tephra					
La Soufrière	EN-46	10 cm	Carey 1992	*G. medarii* foraminifera	600 ± 600
La Soufrière	EN-46	25 cm	Carey 1992	*G. medarii* foraminifera	1600 ± 600
La Soufrière	EN-46	35 cm	Carey 1992	*G. medarii* foraminifera	2200 ± 600
La Soufrière	EN-46	40 cm	Carey 1992	*G. medarii* foraminifera	2500 ± 600
La Soufrière	EN-46	50 cm	Carey 1992	*G. medarii* foraminifera	3100 ± 600
La Soufrière	GS-27	350 cm	Carey 1992	*G. medarii* foraminifera	15,000 ± 400
La Soufrière	EN-46	265 cm	Carey 1992	*G. medarii* foraminifera	15,500 ± 500
La Soufrière	GS-27	415 cm	Carey 1992	*G. medarii* foraminifera	17,600 ± 400
La Soufrière	EN-46	325 cm	Carey 1992	*G. medarii* foraminifera	18,300 ± 500
Lavas					
La Soufrière	**Lower Larikai lava**	**STV_LS_103**	**This study**	**^{40}Ar / ^{39}Ar**	**4.4 ± 4.2 ka**
La Soufrière	**Crater Lava (unit 7)**	**STV_LS_6**	**This study**	**^{40}Ar / ^{39}Ar**	**5.7 ± 4.4 ka**
La Soufrière	**Crater Lava (unit 14)**	**STV_LS_46**	**This study**	**^{40}Ar / ^{39}Ar**	**7.9 ± 7.7 ka**
Morne Garu / La Soufrière	Indian Estate	STV 345	Heath 1997	^{40}Ar / ^{39}Ar	11 ± 14 ka
La Soufrière	**Roseau lava**	**STV_LS_167**	**This study**	**^{40}Ar / ^{39}Ar**	**14.5 ± 3.1 ka**
La Soufrière	**Crater Lava (unit 10)**	**STV_LS_5a**	**This study**	**^{40}Ar / ^{39}Ar**	**25.2 ± 3.8 ka**
La Soufrière	**Roseau lava**	**STV_LS_154**	**This study**	**^{40}Ar / ^{39}Ar**	**31.5 ± 4.1 ka**
La Soufrière	**Lower Larikai lava**	**STV_LS_100**	**This study**	**^{40}Ar / ^{39}Ar**	**33.7 ± 8 ka**
Morne Garu / La Soufrière	Black Point	STV 301	Heath 1997	^{40}Ar / ^{39}Ar	180 ± 21 ka
La Soufrière	South Sandy Bay	STV 323	Heath 1997	^{40}Ar / ^{39}Ar	291 ± 10 ka
La Soufrière	Chain Spout / Rabacca River	STV 358	Heath 1997	^{40}Ar / ^{39}Ar	324 ± 15 ka
La Soufrière	Commantawana Bay	683755	Briden et al., 1979.	K-Ar	360 ± 70 ka
La Soufrière*	**Jacobs well**	**VSG-2**	**This study**	**^{40}Ar / ^{39}Ar**	**475.6 ± 28.3 ka**
La Soufrière	Porter Point	683740	Briden et al., 1979.	K-Ar	660 ± 100 ka
La Soufrière	Rouges Hill (Owia Bay)	683756	Briden et al., 1979.	K-Ar	690 ± 90 ka
Grande Bonhomme	Lowmans Leeward	683741	Briden et al., 1979.	K-Ar	1.16 ± 0.08 Ma
Morne Garu	Richmond Vale	683747	Briden et al., 1979.	K-Ar	1.18 ± 0.10 Ma
Grande Bonhomme	Coulls Hill	683749	Briden et al., 1979.	K-Ar	1.33 ± 0.09 Ma
SE volcanics	Arnos Vale	SV-18	Geothermica Italia / Robertson 2002	K-Ar	1.54 ± 0.62 Ma
SE volcanics	Kingstown / Cane Garden road	683763	Briden et al., 1979	K-Ar	1.65 ± 0.18 Ma
SE volcanics	Villa dyke	SV-29	Geothermica Italia / Robertson 2002	K-Ar	2.50 ± 1.40 Ma
SE volcanics	Calliaqua	683762	Briden et al., 1979	K-Ar	2.49 ± 0.07 Ma
SE volcanics	Windward highway / Prospect corner	683761	Briden et al., 1979	K-Ar	2.74 ± 0.11 Ma

Bold indicates new data presented in this study
GS-27 refers to GILLIS cruise GS7605, core 27; EN-46 refers to ENDEAVOUR cruise EN20
Sample # for marine tephra are base depths of each unit in drill core
* Xenolith